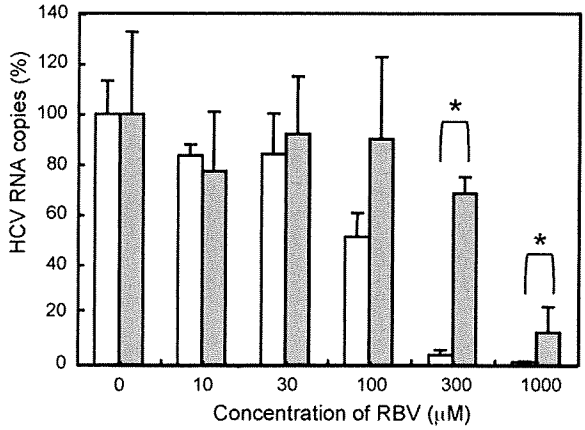

Fig. 1. Inhibitory effect of RBV on HCV RNA levels in genotype 2a replicon cells after long-term treatments with RBV. The replicon cells were serially passaged in 0 or 200 μM RBV for 20 weeks. The cells were then split and incubated with fresh RBV at various concentrations in the absence of G418 for 3 days, followed by the determination of HCV RNA. Clear bars, passage in the absence of RBV: gray bars, passage in the presence of RBV. HCV RNA copies per microgram of total RNA were normalized as percentages of those of untreated (RBV 0 μM). Each data point is presented as the mean of three independent determinations with standard deviation. $^*p < 0.05$.

cells; the EC_{50} values for the variant and wild-type replicon cells were 470 and 102 μM, respectively (Fig. 1). Comparable cytotoxic effects of RBV were observed against wild-type and variant replicon cells, with the CC_{50} (50% cytotoxicity concentration) values of 151 and 156 μM, respectively (data not shown).

3.2. Mapping RBV resistance to cell line or replicon RNA

To test whether reduced susceptibility to RBV in the variant cells observed as above was due to the appearance of mutations within the viral RNA or was cell-derived, total RNAs from the variant and wild-type replicon cells were extracted and used for retransfection of naïve Huh7 cells. Retransfected cells resistant to G418 were established after 4 weeks of cultures in the presence of 1 mg/ml G418 and were assessed for HCV RNA replication sensitivity to RBV (Fig. 2A). HCV RNA levels in the cells obtained from the wild-type replicon were inhibited by 56, 89 and 97% with 100, 300 and 1000 μM RBV, respectively. By contrast, the culture retransfected with RNA derived from the variant replicon cells exhibited inhibition levels of 13, 29 and 89% with the corresponding concentrations of RBV. EC_{50} values were calculated to be 93 and 449 μM, respectively. We confirmed the presence of replicon mutations, as described below, in the cells retransfected with RNA derived from the variant replicon cells.

In order to explore the possibility for cell-derived resistance, both wild-type and variant replicon cells were cured of viral RNAs by IFN treatment; cells were passaged with media containing 100 IU/mL IFN-α in the absence of G418 for 2 months. To compare RBV sensitivity, cured cells were transiently transfected with the wild-type JFH-1 subgenomic replicon RNA and were treated with various concentrations of RBV for 72 h. Similar anti-HCV effects of RBV were observed in the cured cells derived from wild-type and variant replicons, with the EC_{50} values of 147 and 118 μM, respectively (Fig. 2B). Thus, the results suggest that the RBV resistance observed may arise by mutations in the replicon rather than by changes in the cells.

3.3. HCV mutations in replicon variant with reduced susceptibility to RBV

It has been reported that mutations in RNA virus genomes responsible for RBV resistance are mostly present in the coding region for the viral RNA-dependent RNA polymerase (RdRp). On the other hand, it is known that RBV works as an RNA mutagen to generate rapidly mutating viral RNA and that NS5B RdRp and other nonstructural proteins in HCV are involved in the viral replication complex, playing key roles in genome replication. Therefore, we sequenced the coding regions for NS3 through NS5B proteins of the replicon molecules in order to determine whether mutations associated with RBV resistance were generated. As shown in Table 2, there were numerically more synonymous and non-synonymous mutations in the RBV-resistant variant replicon cells (RBV treatment) when compared with untreated replicative conditions (No-treatment) across most regions examined. Mutation frequencies of NS3, NS4B and NS5A regions of RBV treatment were significantly higher than those of No-treatment. The total number of synonymous mutations in the RBV-resistant variant replicon cells was 3 times higher than that under untreated replicative conditions, and the number of non-synonymous mutations in the RBV-resistant variant replicon cells was 1.5 times higher than that under untreated replicative conditions. The number of both synonymous and non-synonymous mutations (NS3, NS4B, NS5A and NS5B regions) in the RBV-resistant replicon cells was greater than that in the control cells. We also found a large number of transition

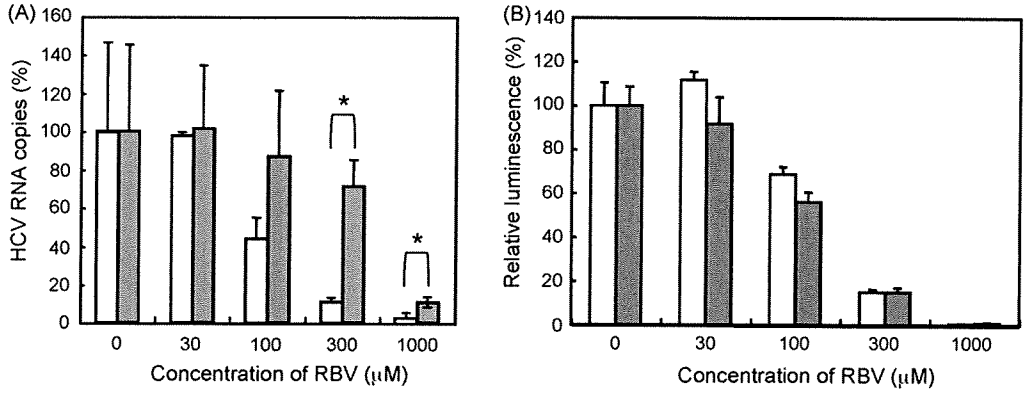

Fig. 2. Testing for replicon-derived resistance (A) or for cell-derived resistance (B). (A) Total RNA from RBV-resistant- or wild-type replicon cells was transfected into naïve Huh7 cells. After selection in 1 mg/ml G418 for 4 weeks, re-established replicon cells, wild-type derived (clear bars) and RBV resistance derived (gray bars), were treated with increasing concentrations of RBV in the absence of G418 for 3 days. HCV RNA copies per microgram total RNA were assessed and the levels from wild-type cells without RBV treatment were set at 100%. Data are indicated as means with standard deviations. $^*p < 0.05$. (B) RBV-resistant- or wild-type replicon cells were cured by passage in IFN-α in the absence of G418. Cured cells were transiently transfected with the replicon RNA derived from pSGR-JFH1/luc. Transient replication assay of transfectants derived from wild-type (clear bars) and RBV resistance (gray bars) was performed after treatment with various concentrations of RBV for 72 h. The values for wild-type-derived cells without RBV treatment were set at 100%. Data are indicated as means with standard deviations.

Table 2
Mutation frequencies in HCV NS regions after 20-weeks culture with or without RBV treatment.

Region	nt length	No-treatment			RBV treatment		
		No. of non-synonymous mutations[a]	No. of synonymous mutations[a]	Mutation frequency (10^{-3})	No. of non-synonymous mutations[a]	No. of synonymous mutations[a]	Mutation frequency (10^{-3})
NS3	1893	1.7 ± 2.1	2.3 ± 1.5	2.1	4.7 ± 2.4	6.5 ± 2.5	5.9[b]
NS4A	165	1.0 ± 1.0	0.3 ± 0.6	8.1	0.3 ± 0.5	0.5 ± 0.9	4.4
NS4B	780	1.3 ± 1.2	0.3 ± 0.6	2.1	2.3 ± 1.5	2.5 ± 1.2	4.7[c]
NS5A	1380	4.0 ± 1.2	2.0 ± 1.2	4.3	5.9 ± 1.2	6.2 ± 2.4	12.2[c]
NS5B	1773	4.5 ± 1.5	2.3 ± 1.5	3.8	4.8 ± 1.8	4.2 ± 1.1	9.0
NS3–NS5B	5991	12.5 ± 2.7	7.3 ± 2.7	–	17.8 ± 4.5	20.1 ± 4.6	–

[a] Values are means ± standard deviations.
[b] $p < 0.05$ relative to No-treatment by the unpaired t-test.
[c] $p < 0.01$ relative to No-treatment by the unpaired t-test.

mutations in RBV-resistant cells, particularly G-to-A and C-to-U transitions, as expected from previous studies. Although mutations were distributed throughout nonstructural regions, four major amino acid substitutions; T1134S in the NS3 region, P1969S in NS4B, V2405A in NS5A, and Y2471H in NS5B, not seen in wild-type cells were observed in most of the subclones among RBV-resistant replicon cells. T1134S, P1969S, V2405A, and Y2471H were present, respectively, in 7 of 11, 6 of 11, 8 of 13, and 7 of 13 PCR subclones sequenced.

3.4. Effects of T1134S, P1969S, V2405A, and Y2471H on RBV susceptibility

To test the possibility that any of the four mutations as identified confer resistance to RBV, we introduced these mutations individually into the JFH-1 subgenomic replicon containing a luciferase reporter gene. Cells transfected with mutant- or wild-type replicon RNA grown in the presence of various concentrations of RBV for 2 or 3 days. As demonstrated in Fig. 3A, the replication levels of all four mutant replicons (SGR-JFH1/Luc-T1134S, -P1969S, -V2405A, and -Y2471H) in the presence of 125 or 500 μM RBV were higher than those of the wild-type replicon. In particular, the Y2471H mutant significantly reduced susceptibility to RBV; replication levels of SGR-JFH1/Luc-Y2471H were 3–5-fold higher when compared to those of wild-type under the present assay conditions.

The relative replication activity of these mutant replicons was further determined in 3-day replication assay without drug treatment (Fig. 3B). All mutant replicons exhibited reduced efficiency relative to the wild-type replicon. Levels of the Y2471H-mutated replicon were approximately 30% of those of the wild-type, thus suggesting that replicon mutants with reduced sensitivity to RBV are associated with decreased replication fitness.

4. Discussion

It is generally accepted that, during chemotherapy against viral infection, high rates of viral replication and high frequencies of mutation lead to generation of drug-resistant mutants. Although several potential mechanisms for the inhibition of HCV replication by RBV have been proposed, the molecular mechanisms involved in the generation of RBV-resistant HCV remain poorly understood.

This study found that long-term treatment of HCV JFH-1-derived replicon cells with RBV leads to selection of preferential mutations in NS3 (T1134S), NS4B (P1969S), NS5A (V2405A) and NS5B (Y2471H) genes. Each mutation only required a single nucleotide change, and P1969S, V2405A and Y2471H are transition mutations, which are known to be commonly caused by incorporated RBV. Site-directed mutagenesis of these mutations into the replicon demonstrated that Y2471H plays a role in reduced susceptibility to RBV.

Crystal structure information revealed that HCV RdRp is organized into an arrangement with palm, fingers, and thumb subdomains (Lesburg et al., 1999). Residue 2471 (the 33rd position of NS5B) is present in the N-terminal loop region that bridges the fingers. Although this site is apparently distant from the active site of the polymerase in the palm region, it has been reported

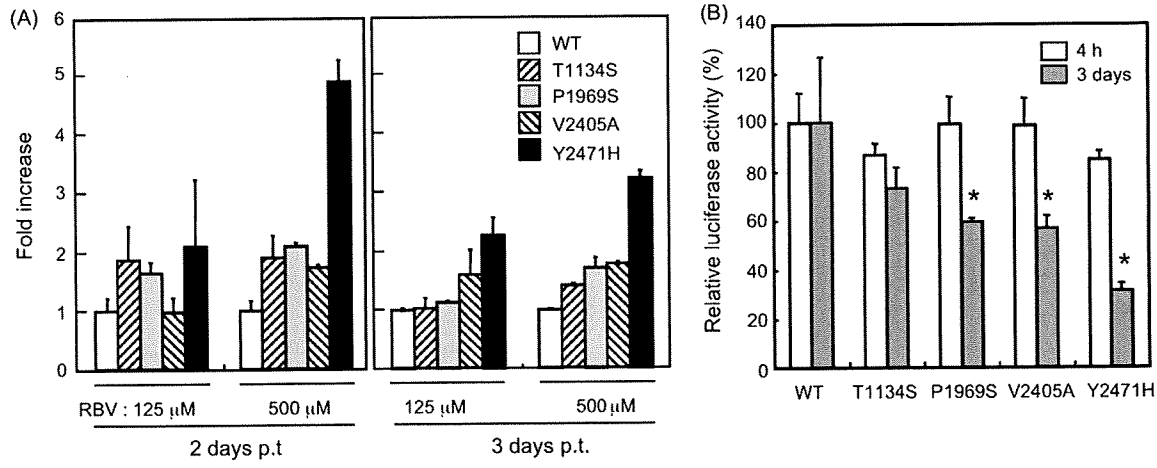

Fig. 3. Impact of major mutations in NS3–NS5B regions on RBV susceptibility (A) and replication capacity (B). Mutated replicons carrying single residue substitutions (T1134S, P1969S, V2405A, and Y2471H) were constructed and used for transient replication assay. Cells were transfected with either wild-type (WT) or with mutant replicon RNA in the absence or presence (125, 500 μM) of RBV. Luciferase activity was assessed at 4 h, 2 days and 3 days post-transfection (p.t.). (A) Luciferase activities of WT were set at 1, and the fold increases in the activities of mutants were plotted. (B) Luciferase activities in the absence of RBV at 4 h and 3 days post-transfection were shown. The activities of mutants were normalized as percentages of the WT activities. Data from triplicate samples were averaged and indicated with standard deviations. *$p < 0.05$ against WT.

that small molecules, such as benzimidazole compounds, are able to specifically bind the fingers-thumb interface and inhibit polymerase activity (Herlihy et al., 2008), thus suggesting that amino acid substitutions in the loop region may affect RNA polymerization. The involvement of tyrosine residue at position 415 of HCV NS5B in RBV resistance has been previously described for patients with genotype 1a infection and for the genotype 1b replicon (Young et al., 2003). Although the mechanism for resistance remains elusive, it has been hypothesized that RBV interacts with RdRp around this residue, which is located in the thumb subdomain, thus affecting RNA polymerization (Young et al., 2003).

Based on analysis of available sequences from Genbank, tyrosine at the 33rd residue of NS5B is conserved in all isolates of genotype 2a, but not in other genotypes. In genotype 1a and 1b isolates, 96% contain histidine and only a small population contains tyrosine or asparagine at the site. All the isolates of genotypes 3, 4, 5 and 6 contain histidine, whereas phenylalanine is conserved for genotype 2b. It should be noted that V2405 and P1969 are also completely conserved for genotype 2a but not for other genotypes. Therefore, it is likely that the identified HCV variants with reduced susceptibility to RBV are genotype-specific. It will be of interest to determine whether HCV genotype 2a is intrinsically more sensitive to RBV when compared with other genotypes.

At present, at least 4 mechanisms of action of RBV are proposed (Lau et al., 2002). They include (1) direct inhibition of the HCV replication machinery, (2) as an RNA mutagen that drives a rapidly mutating RNA virus over the threshold to "error catastrophe", (3) inhibition of the host enzyme inosine monophosphate dehydrogenase (IMPDH), and (4) enhancement of host T-cell-mediated immunity against viral infection. In addition to the direct inhibition, it is also possible that other mechanisms such as error-prone and IMPDH-inhibition are involved in HCV escape from RBV treatment. Further investigation of the interaction of HCV variants with the viral and cellular factors involved in viral resistance may improve understanding of the mechanism(s) of RBV resistance.

In conclusion, RBV encountered resistance from the HCV genotype 2a replicon largely mediated by mutations in the N-terminal region of NS5B. Although whether these mutagenic effects are also demonstrable in IFN-RBV combination therapy will require further studies, the mutations identified in this study represent the first drug-resistant variants belonging to HCV genotype 2a. The drug resistance patterns found in this study may be of benefit in prediction in vivo resistance profiles and the development of next-generation nucleoside analogues as anti-HCV drugs.

Acknowledgments

We thank M. Matsuda, S. Yoshizaki, M. Ikeda, T. Shimoji, M. Kaga and M. Sasaki for their technical assistance. This work was supported by a grant-in-aid for Scientific Research from the Japan Society for the Promotion of Science, from the Ministry of Health, Labour and Welfare of Japan and from the Ministry of Education, Culture, Sports, Science and Technology, and by Research on Health Sciences focusing on Drug Innovation from the Japan Health Sciences Foundation, Japan and by the Program for Promotion of Fundamental Studies in Health Sciences of the National Institute of Biomedical Innovation of Japan. S.S.H. is the recipient of a Research Resident Fellowship from Viral Hepatitis Research Foundation of Japan.

References

Aizaki, H., Nagamori, S., Matsuda, M., Kawakami, H., Hashimoto, O., Ishiko, H., Kawada, M., Matsuura, T., Hasumura, S., Matsuura, Y., Suzuki, T., Miyamura, T., 2003. Production and release of infectious hepatitis C Virus for human liver cell cultures in the three-dimensional radial-flow bioreactor. Virology 314, 16–25.

aus dem Siepen, M., Oniangue-Ndza, C., Wiese, M., Ross, S., Roggendorf, M., Viazov, S., 2007. Interferon-alpha and ribavirin resistance of Huh7 cells transfected with HCV subgenomic replicon. Virus Res. 125, 109–113.

Date, T., Kato, T., Miyamoto, M., Zhao, Z., Yasui, K., Mizokami, M., Wakita, T., 2004. Genotype 2a hepatitis C virus subgenomic replicon can replicate in HepG2 and IMY-N9 cells. J. Biol. Chem. 279, 22371–22376.

Domingo, E., 1996. Biological significance of viral quasispecies. Viral Hep. Rev. 2, 247–261.

Farci, P., Purcell, R.H., 2000. Clinical significance of hepatitis C virus genotypes and quasispecies. Semin. Liver Dis. 20, 103–126.

Forns, X., Purcell, R.H., Bukh, J., 1999. Quasispecies in viral persistence and pathogenesis of hepatitis C virus. Trends Microbiol. 7, 402–410.

Fried, T.R., Bradley, E.H., Towle, V.R., Allore, H., 2002. Understanding the treatment preferences of seriously ill patients. N. Engl. J. Med. 346, 1061–1066.

Herlihy, K.J., Graham, J.P., Kumpf, R., Patick, A.K., Duggal, R., Shi, S.T., 2008. Development of intragenotypic chimeric replicons to determine the broad-spectrum antiviral activities of hepatitis C virus polymerase inhibitors. Antimicrob. Agents Chemother. 52, 3523–3531.

Kato, T., Date, T., Miyamoto, M., Furusaka, A., Tokushige, K., Mizokami, M., Wakita, T., 2003. Efficient replication of the genotype 2a hepatitis C virus subgenomic replicon. Gastroenterology 125, 1808–1817.

Kato, T., Date, T., Miyamoto, M., Sugiyama, M., Tanaka, Y., Orito, E., Ohno, T., Sugihara, K., Hasegawa, I., Fujiwara, K., Ito, K., Ozasa, A., Mizokami, M., Wakita, T., 2005. Detection of anti-hepatitis C virus effects of interferon and ribavirin by a sensitive replicon system. J. Clin. Microbiol. 43, 5679–5684.

Lau, J.Y., Tam, R.C., Liang, T.J., Hong, Z., 2002. Mechanism of action of ribavirin in the combination treatment of chronic HCV infection. Hepatology 35, 1002–1009.

Lesburg, C.A., Cable, M.B., Ferrari, E., Hong, Z., Mannarino, A.F., Weber, P.C., 1999. Crystal structure of the RNA-dependent RNA polymerase from hepatitis C virus reveals a fully encircled active site. Nat. Struct. Biol. 6, 937–943.

Manns, M.P., McHutchison, J.G., Gordon, S.C., Rustgi, V.K., Shiffman, M., Reindollar, R., Goodman, Z.D., Koury, K., Ling, M., Albrecht, J.K., 2001. Peginterferon alfa-2b plus ribavirin compared with interferon alfa-2b plus ribavirin for initial treatment of chronic hepatitis C: a randomised trial. Lancet 358, 958–965.

Martell, M., Esteban, J.I., Quer, J., Genesca, J., Weiner, A., Esteban, R., Guardia, J., Gomez, J., 1992. Hepatitis C virus (HCV) circulates as a population of different but closely related genomes: quasispecies nature of HCV genome distribution. J. Virol. 66, 3225–3229.

Miyamoto, M., Kato, T., Date, T., Mizokami, M., Wakita, T., 2006. Comparison between subgenomic replicons of hepatitis C virus genotypes 2a (JFH-1) and 1b (con1 NK5.1). Intervirology 49, 37–43.

Pfeiffer, J.K., Kirkegaard, K., 2005. RBV resistance in hepatitis C virus replication containing cells conferred by changes in the cell line or mutations in the replicon RNA. J. Virol. 79, 2346–2355.

Simmonds, P., Gallin, J.I., Farrei, A.S., 2000. Hepatitis C virus genotypes. Biomed. Res. Rep. 2, 53–70.

Takeuchi, T., Katsume, A., Tanaka, T., Abe, A., Inoue, K., Tsukiyama Kohara, K., Kawaguchi, R., Tanaka, S., Kohara, M., 1999. Real-time detection system for quantification of Hepatitis C virus genome. Gastroenterology 116, 636–642.

Tanaka, Y., Sakamoto, N., Enomoto, N., Kurosaki, M., Ueda, E., Maekawa, S., Yamashiro, T., Nakagawa, M., Chen, C.-H., Kanazawa, N., Kakinuma, S., 2004. Synergistic inhibition of intracellular hepatitis C virus replication by combination of ribavirin and interferon-alpha. J. Infect. Dis. 189, 1129–1139.

World Health Organization (WHO), 2000. Hepatitis C: global prevalence (update). Weekly Epidemiological Record, WHO 75, 18–19.

Young, K.C., Lindsay, K.L., Lee, K.J., Liu, W.C., He, J.W., Milstein, S.L., Lai, M.M., 2003. Identification of a ribavirin-resistant NS5B mutation of hepatitis C virus during ribavirin monotherapy. Hepatology 38, 869–878.

Zhou, S., Liu, R., Baroudy, B.M., Malcolm, B.A., Reyes, G.R., 2003. The effect of ribavirin and IMPDH inhibitors on hepatitis C virus subgenomic replicon RNA. Virology 310, 333–342.

Biological and immunological characteristics of hepatitis E virus-like particles based on the crystal structure

Tetsuo Yamashita[a,1], Yoshio Mori[a,1], Naoyuki Miyazaki[b,c], R. Holland Cheng[c], Masato Yoshimura[d], Hideaki Unno[e], Ryoichi Shima[a], Kohji Moriishi[a], Tomitake Tsukihara[b], Tian Cheng Li[f], Naokazu Takeda[f], Tatsuo Miyamura[f], and Yoshiharu Matsuura[a,2]

[a]Department of Molecular Virology, Research Institute for Microbial Diseases and [b]Department of Protein Crystallography, Research Institute for Protein Research, Osaka University, Osaka 565-0871, Japan; [c]Department of Molecular and Cellular Biology, University of California, Davis, CA 95616; [d]National Synchrotron Radiation Research Center, 101 Hsin-Ann Road, Hsinchu Science Park, Hsinchu 30076, Taiwan; [e]Department of Applied Chemistry, Faculty of Engineering, Nagasaki University, Nagasaki 852-8521, Japan; and [f]Department of Virology II, National Institute of Infectious Diseases, Tokyo 208-0011, Japan

Edited by Michael G. Rossmann, Purdue University, West Lafayette, IN, and approved June 8, 2009 (received for review April 3, 2009)

Hepatitis E virus (HEV) is a causative agent of acute hepatitis. The crystal structure of HEV-like particles (HEV-LP) consisting of capsid protein was determined at 3.5-Å resolution. The capsid protein exhibited a quite different folding at the protruding and middle domains from the members of the families of *Caliciviridae* and *Tombusviridae*, while the shell domain shared the common folding. Tyr-288 at the 5-fold axis plays key roles in the assembly of HEV-LP, and aromatic amino acid residues are well conserved among the structurally related viruses. Mutational analyses indicated that the protruding domain is involved in the binding to the cells susceptive to HEV infection and has some neutralization epitopes. These structural and biological findings are important for understanding the molecular mechanisms of assembly and entry of HEV and also provide clues in the development of preventive and prophylactic measures for hepatitis E.

capsid | HEV | VLP

Hepatitis E is an acute viral hepatitis caused by infection with hepatitis E virus (HEV) that is transmitted primarily by a fecal-oral route (1, 2). Numerous epidemic and sporadic cases have occurred in developing countries of Asia, the Middle East, and North Africa, where sanitary conditions are not well-maintained. Hepatitis E affects predominantly young adults, and HEV infection in pregnancy is one of the risk factors for severe disease and death (3). Recent epidemiological studies show that significant prevalence of HEV and anti-HEV antibody is found in humans and several animals worldwide, even in developed countries (4–8).

HEV is the sole member of the genus *Hepevirus* within the family *Hepeviridae* and has a 7.2-kb positive-sense RNA genome (9). Five major genotypes have been identified so far (2). The viruses in the genotypes 1 and 2 are maintained among only humans, while those in the genotypes 3 and 4 are found in pigs or wild animals (4–6). However, infections of human with genotypes 3 and 4 via zoonotic transmission or blood transfusion were reported in the developed countries, such as Japan and the United States (7, 8, 10), suggesting that hepatitis E caused by infection with genotypes 3 and 4 of HEV is an important emerging infectious disease. The viruses in the genotype 5 are of avian origin and are thought to be uninfectious to humans (11). The genomic RNA contains three ORFs (ORFs) encoding nonstructural proteins (ORF1), the viral capsid protein composed of 660 amino acids (ORF2) and a small phosphorylated protein of unidentified function (ORF3) (1, 9). The viral capsid protein induces neutralizing antibodies by its immunization (12–15) or during the course of infection (16, 17). A typical signal sequence at the N terminus and 3 potential *N*-glycosylation sites (Asn-X-Ser/Thr) are well-conserved in the capsid protein derived from all mammalian genotypes (18, 19), but the glycosylation status of this protein is still controversial and the biological significance of the modification in the viral life cycle remains unknown. Although propagation of HEV in the cell culture systems reported in earlier studies was not efficient (20–23), Tanaka et al. succeeded in the establishment of a persistent infection system of HEV genotype 3 in human hepatoma (PLC/PRF/5) and human carcinomic alveolar epithelial (A549) cell lines (24). However, sufficient amounts of viral particles cannot be obtained for studies of the structure, life cycle, and pathogenesis of HEV.

Electron microscopy of human stool specimens showed that HEV is a nonenveloped spherical particle with a diameter of approximately 320 Å (25). As an alternative to in vitro propagation of HEV, the baculovirus expression system opens the prospect of studying HEV capsid assembly, since HEV-like particles (HEV-LP) with protruding spikes on the surface can be formed in insect cells infected with a recombinant baculovirus expressing the capsid protein of a genotype 1 strain (26–28). Cryo-electron microscopic (cryoEM) analysis has revealed that HEV-LP is a $T = 1$ icosahedral particle composed of 60 copies of truncated products of ORF2 (27, 28). The HEV-LP appeared to be empty due to a lack of significant density containing RNA inside and was 270 Å in diameter (26–28), which is smaller than the diameter of the native virions. However, the HEV-LP retained the antigenicity and capsid formation of the native HEV particles.

The crystal structures of the recombinant or native $T = 3$ viral particles derived from structurally related mammalian and plant viruses, such as recombinant Norwalk virus (rNV; PDB accession code 1IHM) (29), San Miguel sea lion virus (SMSV; PDB accession code 2GH8) (30), the members of the family *Caliciviridae*, and Carnation mottle virus (CARMV; PDB accession code 1OPO) (31), a member of the family *Tombusviridae*, have

Author contributions: T.Y., Y. Mori, T.T., T.C.L., N.T., T.M., and Y. Matsuura designed research; T.Y., Y. Mori, R.S., K.M., T.C.L., N.T., and Y. Matsuura performed research; T.Y., Y. Mori, N.M., R.H.C., M.Y., and H.U. analyzed data; and T.Y., Y. Mori, and Y. Matsuura wrote the paper.

The authors declare no conflict of interest.

This article is a PNAS Direct Submission.

Data deposition: The atomic coordinates have been deposited in the Protein Data Bank, www.pdb.org (PDB ID code 2ZTN).

[1]T.Y. and Y. Mori contributed equally to this work.

[2]To whom correspondence should be addressed at: Department of Molecular Virology, Research Institute for Microbial Diseases, Osaka University, 3-1 Yamadaoka, Suita-shi, Osaka 565-0871, Japan. E-mail: matsuura@biken.osaka-u.ac.jp.

This article contains supporting information online at www.pnas.org/cgi/content/full/0903699106/DCSupplemental.

www.pnas.org/cgi/doi/10.1073/pnas.0903699106

been determined at resolutions of 3.4 Å, 3.2 Å, and 3.2 Å, respectively. In this study, to understand the structural basis on HEV, we solved the crystal structure of HEV-LP derived from a genotype 3 strain at 3.5-Å resolution and found differences in the folding of the capsid protein among these viruses. On the other hand, we found several structural similarities of shell formation. In particular, it was revealed that aromatic amino acids (Tyr-288 in the case of HEV-LP) at the 5-fold axis play a crucial role in the hydrophobic interaction required for particle formation and are well conserved among these viruses. Furthermore, mutational analyses depicted the putative cellular receptor-binding regions and epitopes for neutralizing of binding (NOB) antibodies on the 3D structure of HEV-LP. The availability of the 3D structure of HEV-LP at high resolution will provide valuable information not only for analyses of the entry and assembly of HEV, but also for the development of a vaccine for hepatitis E.

Results

Preparation of HEV-LP of a Genotype 3. Upon infection with a recombinant baculovirus possessing a genome of the truncated capsid protein (amino acids 112–608) from a genotype 3 strain under the control of polyhedrin promoter, a large amount of HEV-LP was secreted into the culture supernatant as described in the case of HEV-LP of genotype 1 strain (26–28). The purified HEV-LP of genotype 3 was used for further structural and biological analyses.

Overall Structure of HEV-LP. The crystal structure of HEV-LP derived from the genotype 3 strain was determined at 3.5-Å resolution by the molecular replacement method by using a cryoEM map of HEV-LP derived from the genotype 1 strain (27, 28) as an initial phasing model (Fig. 1*A*). As shown in the previous papers (27, 28), HEV-LP shows a $T = 1$ icosahedral symmetry with an external diameter of 270 Å. This particle is composed of 60 subunits of the truncated capsid proteins, forming the icosahedral 2-, 3-, and 5-fold axes. It has 30 protrusions at the 2-fold axis of the surface with large depressions at the 3- and 5-fold axes.

Structure of the HEV Capsid Protein. The truncated HEV capsid protein has 3 definite domains designated as S (shell), M (middle), and P (protruding) composed of the amino acid residues 129–319, 320–455, and 456–606, respectively (Fig. 1*B*). Because the N- and C-terminally truncated capsid proteins were used for the characterization, the typical signal sequence (amino acids 1–22) and following arginine-rich domain (amino acids 23–111) and the C-terminal domain removed by cleavage in insect cells (amino acids 609–660) were not determined in this study. Additionally, the amino acid residues 112–128, 486–487, 555–560, and 607–608 were disordered in this study. The S domain, which forms an internal scaffold structure of the particle, folds into a classical anti-parallel jelly roll-like β-sandwich structure with 8 β-strands (designated as B to I) and 4 short α-helices that are conserved among many viral capsids (Fig. 1*B* and Fig. S1) (29–33). The M domain, which is one of the characteristic domains, has a twisted anti-parallel β-barrel structure composed of 6 β-strands and 4 short α-helices. This domain is tightly associated with the S domain and located on the surface around the icosahedral 3-fold axis (Fig. 1*A* and *B*). The M and P domains are linked with a long proline-rich hinge (amino acids 445–467). Previous studies on the structures of rNV (29) and SMSV (30) revealed that the P domains of the viruses are composed of 2 subdomains, P1 and P2, and the P2 subdomain is located as a large protrusion of the P1 subdomain (Fig. S1). In contrast, the P domain of HEV-LP is composed of a single individual domain forming a twisted anti-parallel β-sheets structure (Fig. 1*B* and Fig. S1), demonstrating that the capsid protein

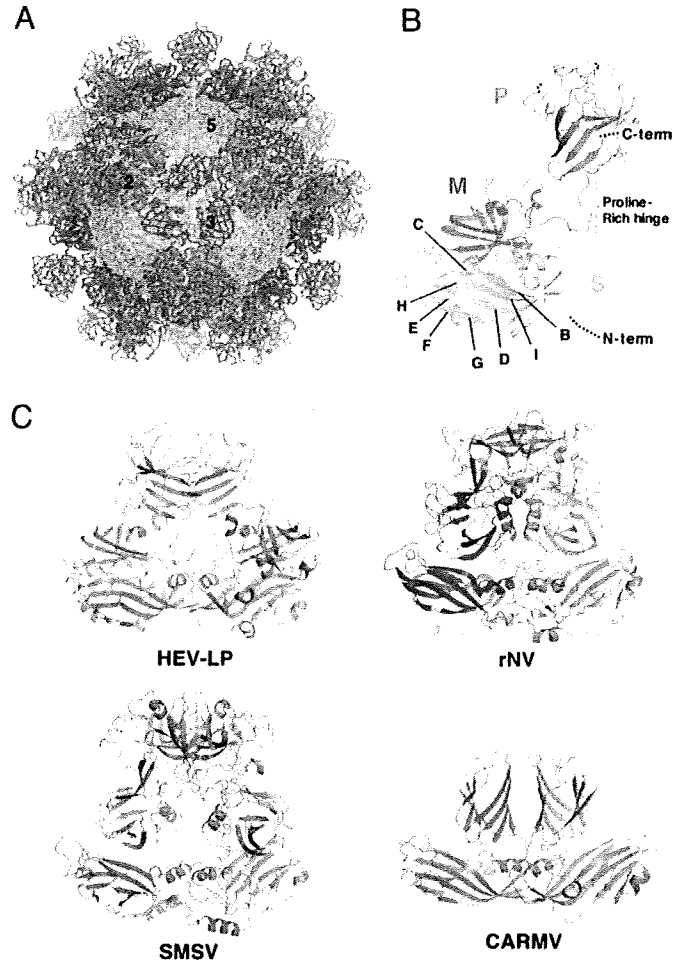

Fig. 1. Crystal structure of HEV-LP and comparison of capsid protein dimers of HEV-LP, rNV, SMSV, and CARMV. The S, M, and P domains of the HEV capsid protein are indicated by pink, green, and blue, respectively. (*A*) HEV-LP is composed of sixty capsid subunits forming icosahedral 2-, 3-, and 5-fold axes and indicating a $T = 1$ symmetry. (*B*) The ribbon diagram of a capsid subunit of HEV-LP (PDB accession code: 2ZTN) shows P, M, and S domains at the top, middle, and bottom, respectively. The disordered regions are shown with dashed lines. The S domain shows a jerry roll-like β-barrel structure conserved in some viruses. The conserved anti-parallel β-strands are indicated (B to I). (*C*) The ribbon diagrams of crystal structures of capsid protein dimers of HEV-LP and those of rNV (PDB accession code 1IHM), SMSV (PDB accession code 2GH8), and CARMV (PDB accession code 1OPO) are indicated. Each capsid protein monomer is colored in red and blue.

of HEV-LP has a significantly different fold from those of caliciviruses, except for the S domain. Although we have no evidence of glycosylation of HEV-LP prepared in insect cells, the HEV capsid protein has 3 potential *N*-glycosylation sites, Asn-137-Leu-Ser, Asn-310-Leu-Thr and Asn-562-Thr-Thr (19). In the dimer structure, the former 2 sites are mapped on the horizontal surface of the S domain, as shown in Fig. S2*A*. However, Asn-137 and Asn-310 are located in the interfaces of the pentamer and trimer structures, respectively (Fig. S2*B* and *C*), suggesting that, if it occurs at all, *N*-glycosylation in these sites may inhibit assembly of HEV-LP. Indeed, Graff et al. (18) reported that HEV carrying mutations in Asn-137 or Asn-310 to Glu lost infectivity to cells or rhesus macaques due to a defect in the virion assembly. On the other hand, Asn-562 is mapped in the central region in the top of the P dimer and exposed in the surface of HEV-LP.

The Dimer Structure at the 2-Fold Axis. It is noteworthy that the HEV-LP dimer at the icosahedral 2-fold axis shows a crossing

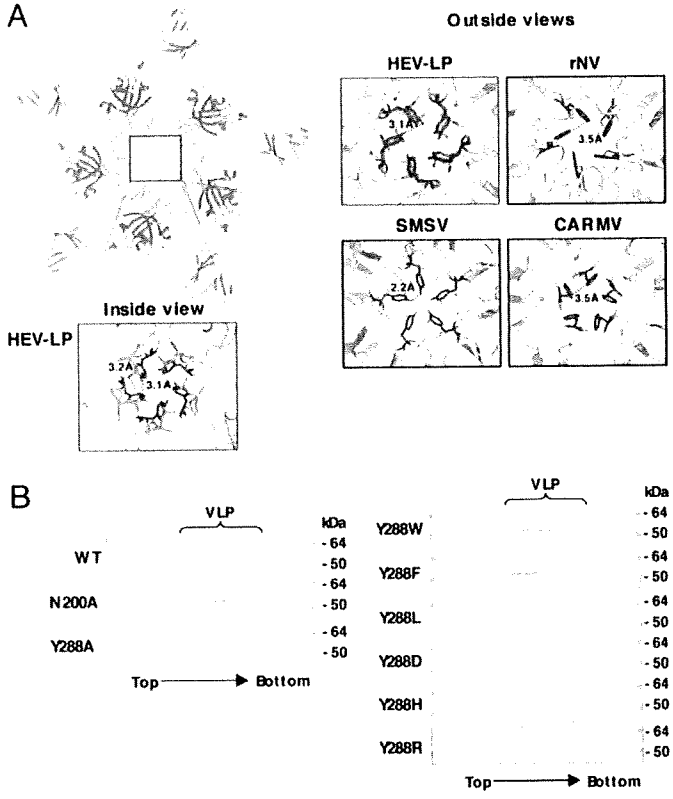

Fig. 2. Interaction of capsid protein subunits of HEV-LP around the 5-fold axis. (*A*) The pentamer of the capsid protein of HEV-LP. The close-up surface diagram of the 5-fold axis showed from outside and inside of HEV-LP. Amino acid residues Asn-200 and Tyr-288 are shown in yellow and green, respectively. The close-up surface diagram of the 5-fold axis showed from outside of rNV, SMSV, and CARMV. The aromatic amino acids Phe-118 of rNV, Tyr-330 of SMSV, and Phe-145 of CARMV are indicated in green. The deduced interacting atoms are connected with dashed lines, and the distances are indicated. (*B*) Sucrose density fractionation assay using the wild-type or mutant capsid proteins (53 kDa) in which the amino acids composing the 5-fold axis were substituted. The capsid protein composing HEV-LP was found in the 5–9th fractions from the top, while that which failed to form particles was found in the top fractions. The molecular mass of approximately 64 kDa was a non-specific protein.

topology of the P versus M and S domains, while that of the other viruses with protrusions at the 2-fold axis, containing rNV, SMSV, and CARMV, exhibits a parallel topology of each domain (Fig. 1*C*). The flexibility of the long proline-rich hinge region between the M and P domains allows this unique topology of HEV-LP. The P domain of HEV-LP interacts with not only the P domain but also the M domain of the counterpart to stabilize the dimer structure. Despite these topological differences, the overall structure of the protrusion dimeric structure at the 2-fold axis is similar to that of rNV and SMSV. The disordered residues 486–487 and 555–560 are located in the apical region of the protrusion, suggesting that this region is flexible to take advantage of the interaction with other molecules.

Five-Fold Axis Packaging. The inter-molecule-interface of the capsid pentamer at the icosahedral 5-fold axis is composed of only S domains, and these interaction regions are narrower than those of the dimer and trimer at the 2-fold and 3-fold axes, respectively (Fig. 2*A*), suggesting that the pentamer formation is a key step of HEV-LP assembly. There are 4 loops between the β-sheets in the S domain, designated as loops B–C (amino acids 139–152), D–E (amino acids 196–206), F–G (amino acids 236–241), and H–I (amino acids 281–296), around the center of the pentamer structure. Among them, the loops B–C and F–G are not in close proximity to the next subunits, suggesting they are not implicated in the inter-molecular interaction. In contrast, loops D–E and H–I do interact with the next subunits. In particular, the side chains of Asn-200 and Tyr-288 in loops D–E and H–I, respectively, interact with those of the next subunits, from which they are separated by a distance of approximately 3.2 Å, filling in the central pore (Fig. 2*A*). These observations led us to hypothesize that these amino acid residues are important for assembly and stability of the particles. To examine this hypothesis, we constructed 2 mutant capsid proteins in which Asn-200 was replaced with alanine (N200A) or Tyr-288 was replaced with alanine (Y288A), and the effect of these mutations on the particle formation was determined by a density-fractionation assay (Fig. 2*B*). Comparative amounts of the mutant proteins to the wild-type capsid were expressed and released into the supernatants of cells infected with the recombinant baculoviruses. N200A but not Y288A formed VLP as the wild-type, indicating that Tyr-288 plays a more crucial role in particle formation than Asn-200. The aromatic amino acids, Phe-118, Tyr-330, and Phe-145, are also found in the icosahedral 5-fold axis of rNV, SMSV, and CARMV, respectively (Fig. 2*A*). To examine the role of the aromatic side chain in Tyr-288 in the particle formation, a series of mutants in which Tyr-288 was replaced with tryptophan, phenylalanine, leucine, asparatic acid, histidine, or arginine (Y288W, Y288F, Y288L, Y288D, Y288H, or Y288R) were generated. All of them were expressed and released into the culture medium, as well as was the wild type. The mutants with aromatic amino acids, Y288W and Y288F, were able to form HEV-LP, whereas other mutants produced no or very few particles (Fig. 2*B*). These results suggest that the aromatic side chain of Tyr-288 plays a crucial role in the HEV-LP formation by shutting off the central pore of the pentamer, and that the aromatic amino acids in the positions corresponding to Tyr-288 of HEV are functionally conserved among the structurally related viruses.

Binding of HEV-LP to Cultured Cells. The early steps of HEV entry remain unclear because of the lack of a robust cell culture system for HEV, despite recent progress in the in vitro propagation of HEV in the cell lines PLC/PRF/5 and A549 (24). HEV-LP was able to bind to several cell lines, including PLC/PRF/5 and A549 cells, but not to mouse myeloma P3 × 63Ag8U.1 (P3U1) cells (Fig. S3), suggesting that a binding assay using HEV-LP is useful to examine the first step of receptor-binding of HEV to the target cells. Among the cell lines examined, the human hepatoma cell line Huh7, exhibited a greater ability to bind to HEV-LP than the cell lines PLC/PRF/5 and A549. Therefore, Huh7 cells were used for the following binding experiments of HEV-LP.

Three-Dimensional Mapping of Epitopes for NOB Antibodies. We examined the ability of the 10 newly produced anti-HEV-LP monoclonal antibodies to inhibit the binding of HEV-LP to Huh7 cells (Fig. 3*A*). Two of the monoclonal antibodies, MAB1323 and MAB272, exhibited NOB of HEV-LP to Huh7 cells and recognized the P domain by immunoblotting using the GST (GST)-fused HEV capsid proteins (Fig. S4). However, further truncation of the C-terminal 28 or N-terminal 24 amino acids from the GST-fused P domain abrogated the binding with the antibodies, indicating that it is difficult to determine the epitopes of the antibodies in more detail using a series of truncated mutants of the P domain. A competitive enzyme-linked immunosorbent assay (ELISA) suggested that MAB1323, MAB272, and MAB161, but not MAB358, which was used as a detector in the binding assay, recognized the same or adjacent epitopes (Fig. S5). The P domains of rNV and feline calicivirus were suggested to be involved in the binding to the receptor molecules (34–36), and we therefore hypothesized that the P

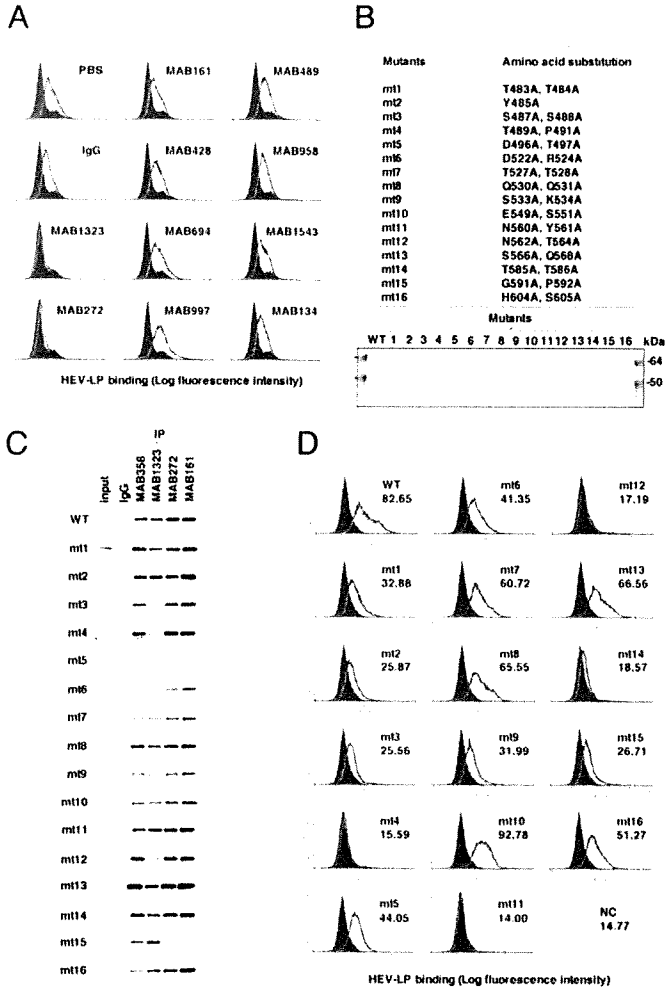

Fig. 3. Characterization of monoclonal antibodies and mutant HEV-LPs. (*A*) Neutralization of binding (NOB) of HEV-LP to Huh7 cells by monoclonal antibodies to HEV-LP. After preincubation of HEV-LP (10 μg/mL) with each of the monoclonal antibodies (20 μg/mL) for 1 h at 37°C, the mixture was inoculated into Huh7 cells and incubated for 1 h at 4°C. HEV-LP (lined area) bound to cells was detected by flow cytometry. The filled area indicates mock-incubated cells. (*B*) Construction of HEV-LP mutants. Sixteen HEV-LP mutants, in which the surface amino acid residues of the P domain were substituted, were constructed. The protein bands of 100 ng each of the purified wild-type and mutant HEV-LPs were visualized by Coomassie brilliant blue staining after SDS/PAGE. (*C*) Reactivities of NOB antibodies with the mutant HEV-LPs. Immunoprecipitation analyses of a series of HEV-LPs by NOB (MAB1323 and MAB272) or non-NOB antibodies (MAB358 and MAB161). Immunoprecipitated HEV-LPs were detected by an anti-HEV capsid rabbit polyclonal antibody. (*D*) Binding capability of the mutant HEV-LPs to Huh7 cells. Wild-type or mutant HEV-LPs (10 μg/mL) were incubated with Huh7 cells for 1 h at 4°C, and then HEV-LP (lined area) bound to cells was detected by flow cytometry. The filled area indicates mock-incubated cells. The MFI is shown in each panel.

domain of HEV-LP might also be involved in the cell binding. To examine this possibility, we prepared 16 HEV-LP mutants in which 1 or 2 amino acid residues at the surface of the P domain were substituted (Fig. 3*B*). The density fractionation assay indicated that all of the mutant proteins formed HEV-LP in the manner of the wild-type capsid protein. MAB358, which recognized an epitope on the M domain (Fig. S4), was capable of precipitating all of the mutants (Fig. 3*C*). MAB1323 exhibited no interaction with mt3 and a weak precipitation of mt4 and mt12. Both MAB272 and MAB161 exhibited no or weak precipitation of mt5 and mt15, whereas MAB272 but not MAB161 exhibited

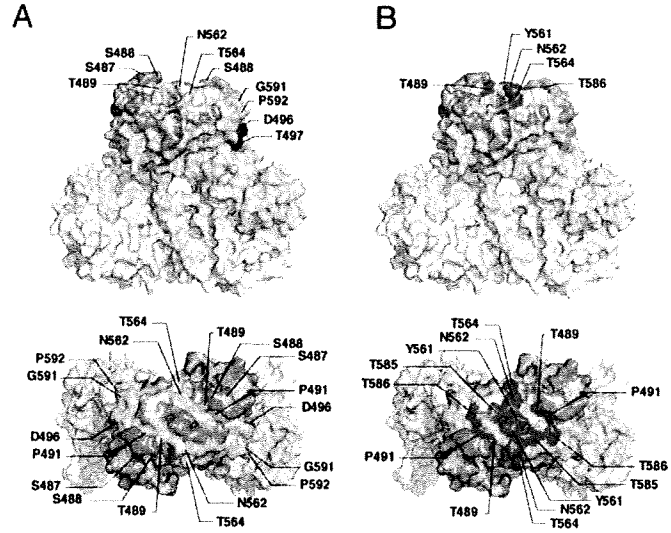

Fig. 4. Amino acid residues involved in the recognition by NOB antibodies and in the binding to Huh7 cells. Surface diagrams of the capsid protein dimer from a lateral (*Upper*) or top (*Lower*) view. (*A*) Amino acids in HEV-LP involved in the complete loss (deep color) or reduction (light color) of reactivity to MAB1323 and MAB272 are shown in orange and green, respectively. (*B*) Amino acids in HEV-LP responsible for binding to Huh7 cells are shown in red. Domains S, M, and P are colored pink, blue and gray, respectively. The substitutions in the P domain of HEV-LP that exhibited no effect on the reactivity with NOB antibodies or the binding to Huh7 cells are shown in dark gray.

NOB of HEV-LP to Huh7 cells (Fig. 3*A* and *C*). The substituted amino acids of these mutants are illustrated in the 3D structure of the capsid dimer (Fig. 4*A*), and these results suggest that the NOB antibodies MAB1323 and MAB272 recognize the peripheral region of the apical surface (orange) and the horizontal region (green) of the P domain above the M domain at the 3-fold axis, respectively.

Three-Dimensional Mapping of a Region Crucial for Binding to the Target Cells. To determine the region important for binding to the cell surface, the mutant HEV-LPs substituted into the P domain were also used in the assay of binding to Huh7 cells (Fig. 3*D*). The wild-type HEV-LP bound to Huh7 cells with a geographic mean fluorescence intensity (MFI) of 82.65. Among the mutants examined, mt4, mt11, mt12, and mt14 exhibited significantly low MFI values of less than 20. Similar results were obtained using A549 cells (Fig. S6). The amino acid residues required for cell binding were mapped in the central flexible region of the apical surface as shown in Fig. 4*B* (red). This region is partially overlapped with epitopes of MAB1323 (Fig. 4*A*) and other neutralizing antibodies reported by Schofield et al. (16) as shown in Fig. S7. These results suggested that the apical center region of the P domain is involved in the association with not-yet-identified cellular receptor(s).

Discussion

The expression of the truncated HEV capsid protein (amino acids 112–608) in insect cells resulted in assembly of HEV-LP, which retains an antigenicity similar to that of the native HEV particles (26, 37). This particle with a $T = 1$ symmetry has a diameter of 270 Å, which is smaller than the 320-Å diameter of the native virion detected in the fecal specimens of patients (25). It has been reported that the interior cavity of HEV-LP is too small to accommodate a viral RNA of 7.8 kb in length (28) and that the particles show no evidence of nucleotide contents (26, 28). Therefore, native HEV particles are sug-

Table 1. Data collection and processing statistics for HEV-LP

Data collection	
Space group	$P2_12_12_1$
Cell dimensions	
a, *b*, *c*, Å	336.8, 349.4, 359.5
X-ray wavelength, Å	1.0000
Resolution, Å	50–3.55 (3.68–3.55)
R_{merge}*	0.131 (0.498)
$I/\sigma I$	9.8 (3.2)
Completeness, %	99.9 (99.8)
Redundancy	5.6 (5.2)
Refinement	
Resolution range, Å	20–3.56
No. reflections	494,466
R_{work}/R_{free}	30.5/30.9
No. atoms	
Protein	215,400
B factors	
Protein	94.9
rmsd	
Bond length, Å	0.009
Bond angle, °	1.355

Values in square brackets refer to the highest-resolution shell.
*$R_{merge} = \Sigma_{hkl}\Sigma_i|I(hkl)_i - \langle I(hkl)\rangle|/\Sigma_{hkl}I(hkl)$, where $I(hkl)_i$ is the ith measurement of the intensity of reflection hkl and $\langle I(hkl)\rangle$ is the mean intensity of reflection *hkl*.

gested to be composed of a larger number and/or a larger size of capsid proteins than HEV-LP. In some cases of plant viruses with a $T = 3$ symmetry, the capsid proteins assembled into particles with a $T = 1$ symmetry by deletion of the N-terminal basic region (38, 39) or amino acid substitutions either in the N-terminal region or in the linker domain between the N-terminal region and S domain (39), suggesting that the N-terminal basic region plays an important role in switching of the transition from $T = 3$ to $T = 1$ symmetry. In addition, expression of the NV capsid protein in insect cells resulted in production of not only $T = 3$ large particles but also small particles thought to have the $T = 1$ symmetry (40). Based on many similarities of the capsid structures and their packaging of structurally related viruses, the native HEV particles are suggested to possess a $T = 3$ surface lattice. The flexibility of the proline-rich hinge linking the M and P domains could allow the capsid protein dimer to switch conformations between the A/B and C/C subunits found in $T = 3$ viruses. Although structure of the native HEV may be slightly different from that of the HEV-LP, the data obtained in this study by using HEV-LP should provide useful information to understand the structure of viral particle, life cycle, and pathogenesis of HEV. The S domain shares the jellyroll fold with some other icosahedral viruses (29–33). It was found that the capsid proteins with substitutions of Tyr-288 positioned at the center of the pentamer structure built in interS domain-interaction failed to assemble into HEV-LP. Alignment analysis of amino acid sequences using data available in GeneBank showed that Tyr-288 is completely conserved within 5 genotypes of HEV. Furthermore, residues corresponding to Tyr-288 of the HEV capsid protein are found in the structures of rNV (Phe-118), SMSV (Tyr-330), and CARMV (Phe-145), although the positions of these aromatic residues are different. Tyr-288 of HEV and Tyr-330 of SMSV located in the H-I loop and Phe-110 of rNV in the D–E loop are exposed at the outside surface of the particles, whereas Phe-145 of CARMV located in the D–E loop is exposed at the interior of the particle. These data suggest that the aromatic side chains of these residues are involved in hydrophobic interactions with those of the next subunits, assuring stable assembly of the particles. During entry into cells, rearrangement of the virion structure is required for release of the genome from the shell. However, the entry and uncoating mechanisms of HEV remain unknown. Because the center of the pentamer is the thinnest region of the particle and takes a channel-like structure (28), this region might also be important for uncoating and release of the viral RNA. It has been proposed that the 5-fold axis of poliovirus is involved in the genomic RNA translocation via conformational change of the virion initiated by binding to the receptor molecules (41, 42).

The first step in viral entry into a target cell is binding to the cellular receptors. The human hepatoma PLC/PRF/5 and lung epithelial A549 cell lines, which are highly susceptible to persistent HEV-infection (24), are likely to express functional HEV receptors on the cell surface. However, HEV-LP had reduced binding to these cells compared to the other cell lines examined. Therefore, the human hepatoma cell line Huh7, which also exhibited a susceptibility to HEV infection (13, 18) and readily bound to HEV-LP, was mainly used in this study. It has been reported that the P domains of noroviruses and the feline calicivirus were involved in the binding to the putative receptors, histo-blood antigens (35, 36) and the feline junctional adhesion molecule (34), respectively. The peptide of the HEV capsid protein (amino acids 368–606), which consists of a part of the M and an entire P domain, was shown to be capable of binding to several cell lines (13), suggesting that the P domain of HEV is also involved in the binding to the cell receptors. Indeed, the mutational analyses in this study indicated that the central flexible region of the top of the P domain of HEV-LP plays a crucial role for binding to Huh7 and A549 cells. This is consistent with a recent study by Graff et al. in which an N562Q mutant of HEV lost infectivity to culture cells and rhesus macaques despite the production of viral particles (18). Interestingly, a possible *N*-glycosylation site, Asn-562-Thr-Thr, is mapped in this region. *N*-glycosylation is an unusual posttranslational modification for nonenveloped viruses, except for rotaviruses (43). The mutant capsid mt12, which has substitutions of Asn-562 and Thr-564 to alanine, exhibited the same migration as the wild-type protein in SDS/PAGE, suggesting that the HEV-LP produced in insect cells was not glycosylated at Asn-562. Lack of *N*-glycosylation in the capsid protein has also been reported in mammalian cells infected with HEV (18), whereas some portion of the capsid protein was glycosylated and transported to the cell surface upon overexpression in mammalian cells (19). *N*-glycosylation of the HEV capsid at Asn-562 may have a negative effect on the receptor-binding, whereas it may play a positive role in other functions, including pathogenesis. The biological significance of the glycosylation of HEV capsid protein remains to be studied.

Although there is currently a lack of sensitive and reliable assays to determine the neutralizing activity of anti-HEV antibodies, the assay of NOB of HEV-LP binding to the target cells is thought to be a suitable alternative method. Measurement of the reactivity of a panel of mutant HEV-LPs revealed that the epitopes of MAB1323 and MAB272 antibodies are mapped in the peripheral region of the apical surface and the horizontal region of the P domain dimer, respectively. These results further support the notion that the P domain of HEV-LP is important for the binding to cells. MAB1323 is suggested to directly inhibit the interaction between HEV-LP and cellular receptors through binding to the apical surface, whereas MAB272 may have an allosteric effect, inducing conformational change of the P domain through binding to the horizontal region. A number of monoclonal antibodies are capable of neutralizing in vitro and in vivo infection of HEV (12–17), and many of them recognize conformational epitopes

of the capsid protein, as seen in the MAB1323 and MAB272 antibodies prepared in this study. Monoclonal antibodies against linear epitopes located in amino acids 578–607 of a genotype 1 capsid protein (16) were overlapped with a part of the putative receptor-binding domain and the epitope of MAB272, supporting the data of the present study. On the other hand, monoclonal antibodies against the linear epitopes located in amino acids 423–438 and amino acids 423–443 in the M domain of a genotype 1 capsid protein neutralized binding of a peptide derived from the capsid protein to cells and HEV-infection (13), suggesting the importance of the M domain in the binding step.

In summary, we have determined the crystal structure of HEV-LP produced in insect cells and demonstrated its structural characteristics in comparison with the structurally related animal and plant viruses. This study will provide useful information for elucidation of the molecular mechanisms of HEV-life cycles and for the development of prophylactic and therapeutic measures for hepatitis E.

Materials and Methods

Expression, Purification, and Crystallization of HEV-LP. The recombinant baculovirus encoding the ORF2 of the HEV genotype 3, 2712 strain was expressed in insect cells. HEV-LP was purified as described previously (28) and crystallized by the hanging-drop vapor-diffusion method. Details are reported in *SI Materials and Methods*.

Data Collection and Phase Determination. x-ray diffraction data were collected at 100 K on beamlines BL17A at the Photon Factory (KEK). The statistics of X-ray diffraction data collection are summarized in Table 1. The solved 3D structure of HEV-LP was submitted to the Protein Data Bank under the PDB accession code of 2ZTN. Details are reported in *SI Materials and Methods*.

ACKNOWLEDGMENTS. We thank H. Murase for her secretarial work and the staff of SPring-8 BL44XU beamline and synchrotron beamline NW-17A of the Photon Factory, High Energy Accelerator Research Organization for their assistance with the data collection. This work was supported in part by grants-in-aid from the Research and Development Program for New Bio-industry Initiatives of Bio-oriented Technology Research Advancement Institution (BRAIN) and the Foundation for Research Collaboration Center on Emerging and Re-emerging Infections.

1. Panda SK, Thakral D, Rehman S (2007) Hepatitis E virus. *Rev Med Virol* 17:151–180.
2. Purcell RH, Emerson SU (2008) Hepatitis E: An emerging awareness of an old disease. *J Hepatol* 48:494–503.
3. Navaneethan U, Al Mohajer M, Shata MT (2008) Hepatitis E and pregnancy: Understanding the pathogenesis. *Liver Int* 28:1190–1199.
4. Meng XJ, *et al.* (1997) A novel virus in swine is closely related to the human hepatitis E virus. *Proc Natl Acad Sci USA* 94:9860–9865.
5. Sonoda H, *et al.* (2004) Prevalence of hepatitis E virus (HEV) infection in wild boars and deer and genetic identification of a genotype 3 HEV from a boar in Japan. *J Clin Microbiol* 42:5371–5374.
6. Okamoto H (2007) Genetic variability and evolution of hepatitis E virus. *Virus Res* 127:216–228.
7. Li TC, *et al.* (2005) Hepatitis E virus transmission from wild boar meat. *Emerg Infect Dis* 11:1958–1960.
8. Yazaki Y, *et al.* (2003) Sporadic acute or fulminant hepatitis E in Hokkaido, Japan, may be food-borne, as suggested by the presence of hepatitis E virus in pig liver as food. *J Gen Virol* 84:2351–2357.
9. Tam AW, *et al.* (1991) Hepatitis E virus (HEV): Molecular cloning and sequencing of the full-length viral genome. *Virology* 185:120–131.
10. Matsubayashi K, *et al.* (2004) Transfusion-transmitted hepatitis E caused by apparently indigenous hepatitis E virus strain in Hokkaido, Japan. *Transfusion* 44:934–940.
11. Huang FF, *et al.* (2004) Determination and analysis of the complete genomic sequence of avian hepatitis E virus (avian HEV) and attempts to infect rhesus monkeys with avian HEV. *J Gen Virol* 85:1609–1618.
12. Emerson SU, *et al.* (2006) Putative neutralization epitopes and broad cross-genotype neutralization of Hepatitis E virus confirmed by a quantitative cell-culture assay. *J Gen Virol* 87:697–704.
13. He S, *et al.* (2008) Putative receptor-binding sites of hepatitis E virus. *J Gen Virol* 89:245–249.
14. Meng J, *et al.* (2001) Identification and characterization of the neutralization epitope(s) of the hepatitis E virus. *Virology* 288:203–211.
15. Takahashi M, *et al.* (2008) Production of monoclonal antibodies against hepatitis E virus capsid protein and evaluation of their neutralizing activity in a cell culture system. *Arch Virol* 153:657–666.
16. Schofield DJ, Glamann J, Emerson SU, Purcell RH (2000) Identification by phage display and characterization of two neutralizing chimpanzee monoclonal antibodies to the hepatitis E virus capsid protein. *J Virol* 74:5548–5555.
17. Schofield DJ, Purcell RH, Nguyen HT, Emerson SU (2003) Monoclonal antibodies that neutralize HEV recognize an antigenic site at the carboxyterminus of an ORF2 protein vaccine. *Vaccine* 22:257–267.
18. Graff J, *et al.* (2008) Mutations within potential glycosylation sites in the capsid protein of hepatitis E virus prevent the formation of infectious virus particles. *J Virol* 82:1185–1194.
19. Zafrullah M, Ozdener MH, Kumar R, Panda SK, Jameel S (1999) Mutational analysis of glycosylation, membrane translocation, and cell surface expression of the hepatitis E virus ORF2 protein. *J Virol* 73:4074–4082.
20. Huang R, *et al.* (1999) Cell culture of sporadic hepatitis E virus in China. *Clin Diagn Lab Immunol* 6:729–733.
21. Kazachkov Yu A, *et al.* (1992) Hepatitis E virus in cultivated cells. *Arch Virol* 127:399–402.
22. Meng J, Dubreuil P, Pillot J (1997) A new PCR-based seroneutralization assay in cell culture for diagnosis of hepatitis E. *J Clin Microbiol* 35:1373–1377.
23. Tam AW, *et al.* (1997) In vitro infection and replication of hepatitis E virus in primary cynomolgus macaque hepatocytes. *Virology* 238:94–102.
24. Tanaka T, Takahashi M, Kusano E, Okamoto H (2007) Development and evaluation of an efficient cell-culture system for Hepatitis E virus. *J Gen Virol* 88:903–911.
25. Bradley D, *et al.* (1988) Aetiological agent of enterically transmitted non-A, non-B hepatitis. *J Gen Virol* 69:731–738.
26. Li TC, *et al.* (1997) Expression and self-assembly of empty virus-like particles of hepatitis E virus. *J Virol* 71:7207–7213.
27. Li TC, *et al.* (2005) Essential elements of the capsid protein for self-assembly into empty virus-like particles of hepatitis E virus. *J Virol* 79:12999–13006.
28. Xing L, *et al.* (1999) Recombinant hepatitis E capsid protein self-assembles into a dual-domain T = 1 particle presenting native virus epitopes. *Virology* 265:35–45.
29. Prasad BV, *et al.* (1999) X-ray crystallographic structure of the Norwalk virus capsid. *Science* 286:287–290.
30. Chen R, Neill JD, Estes MK, Prasad BV (2006) X-ray structure of a native calicivirus: Structural insights into antigenic diversity and host specificity. *Proc Natl Acad Sci USA* 103:8048–8053.
31. Morgunova E, *et al.* (1994) The atomic structure of Carnation Mottle Virus capsid protein. *FEBS Lett* 338:267–271.
32. Hogle JM, Chow M, Filman DJ (1985) Three-dimensional structure of poliovirus at 2.9 A resolution. *Science* 229:1358–1365.
33. Tsao J, *et al.* (1991) The three-dimensional structure of canine parvovirus and its functional implications. *Science* 251:1456–1464.
34. Bhella D, Gatherer D, Chaudhry Y, Pink R, Goodfellow IG (2008) Structural insights into calicivirus attachment and uncoating. *J Virol* 82:8051–8058.
35. Bu W, *et al.* (2008) Structural basis for the receptor binding specificity of Norwalk virus. *J Virol* 82:5340–5347.
36. Choi JM, Hutson AM, Estes MK, Prasad BV (2008) Atomic resolution structural characterization of recognition of histo-blood group antigens by Norwalk virus. *Proc Natl Acad Sci USA* 105:9175–9180.
37. Li TC, *et al.* (2004) Protection of cynomolgus monkeys against HEV infection by oral administration of recombinant hepatitis E virus-like particles. *Vaccine* 22:370–377.
38. Hsu C, *et al.* (2006) Characterization of polymorphism displayed by the coat protein mutants of tomato bushy stunt virus. *Virology* 349:222–229.
39. Kakani K, Reade R, Katpally U, Smith T, Rochon D (2008) Induction of particle polymorphism by cucumber necrosis virus coat protein mutants in vivo. *J Virol* 82:1547–1557.
40. White LJ, Hardy ME, Estes MK (1997) Biochemical characterization of a smaller form of recombinant Norwalk virus capsids assembled in insect cells. *J Virol* 71:8066–8072.
41. Belnap DM, *et al.* (2000) Molecular tectonic model of virus structural transitions: The putative cell entry states of poliovirus. *J Virol* 74:1342–1354.
42. Bubeck D, Filman DJ, Hogle JM (2005) Cryo-electron microscopy reconstruction of a poliovirus-receptor-membrane complex. *Nat Struct Mol Biol* 12:615–618.
43. Jayaram H, Estes MK, Prasad BV (2004) Emerging themes in rotavirus cell entry, genome organization, transcription and replication. *Virus Res* 101:67–81.

人獣共通感染症

清水実嗣 監修

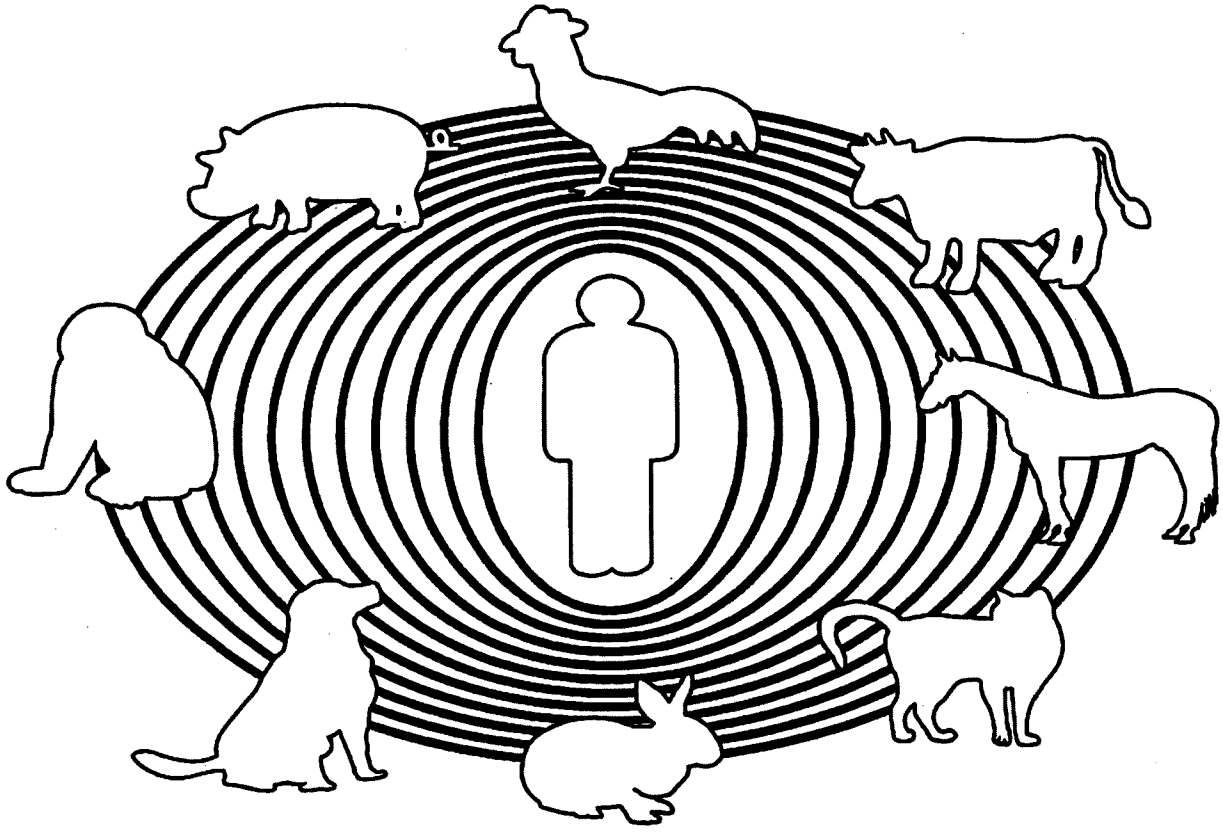

養賢堂

第６章　Ｅ型肝炎

１．はじめに

Ｅ型肝炎はＥ型肝炎ウイルス（HEV）の感染によって起こるヒトの急性肝炎である．最近まで，本病は衛生状態の悪い発展途上国に限って発生が確認されていたため，欧米や日本などの先進国では輸入感染症（旅行者感染症）と考えられてきた．しかし，近年，日本を含む先進国で海外渡航歴のないヒトでの本病の発生が報告され，また，日本の国民20人に1人がHEVに対する抗体を保有していることも明らかにされた．これらのことから，先進国でもHEVが土着していると考えられるようになり，その感染ルートに関心が集まってきた．一方，ブタにはヒト由来HEVと遺伝学的に酷似したHEVが広く浸淫していること，ブタ以外の幾つかの動物においてもHEVあるいはHEV様ウイルスが存在することが近年わかってきた．このような中で，2003年には動物（食肉）からヒトに感染してＥ型肝炎を発症させたとする直接的あるいは間接的な証拠が相次いで報告された．すなわち，Ｅ型肝炎は人獣共通感染症としての側面を有することが明らかにされた．しかし，動物からヒトへの感染はどの程度の頻度で起こっているのか，現時点では全く不明である．また，Ｅ型肝炎の発生が近年先進国で急増している事実は認められていない．

２．疫学と臨床症状

ヒトの主要なウイルス性肝炎としてＡ，Ｂ，Ｃ，ＤおよびＥ型が知られている．この中で，Ｅ型肝炎は衛生状態の悪いアジアにおける流行性肝炎の最も重要な疾病である．伝播は主にヒト糞便中に排泄されたウイルスの経口感染（糞口ルート）によるもので，とくに水系伝播（water-borne transmission）が多いとされる．大規模な発生としては，1955年インドのニューデリーにおいて飲用上水の糞便汚染が原因で29,000人が発症した．その後，同様な感染ルートによる大流行がミャンマー（1976～1977年；20,000人発症；妊婦において18％の致死率），インドのカシミール（1978年；52,000人発症），中国（1986～1988年；100,000人発症），ソマリア（1988～1989年；11,000人発症），メキシコ（1988～1989年；4,000人発症）などで確認されている．最近（2004年）では，アフリカのチャドやスーダンで大流行が確認されている．また，これらの国々では散発的な発生も頻繁に認められる．症例の多くは青年や大人であり，小児での発症例は少ない．患者から家族内接触者などへの二次罹患率は低く，その理由としては糞便中に排泄されるウイルス量が少ないことが上げられる．致死率は1～3％とＡ型肝炎の約10倍であり，とくに，妊婦は重症化しやすく，妊娠第三期での致死率は15％～25％と非常に高いことが報告されている．

潜伏期は2～9週間（平均6週間）で，臨床症状はＡ型肝炎と似ており，腹痛，食欲不振，

褐色尿を伴った黄疸，発熱，肝臓の腫脹，不快感，嘔吐などで，時に関節痛，下痢，蕁麻疹なども見られる．黄疸症状が約2週間続いた後，通常発症から1カ月を経て完治する．黄疸に先立ってウイルス血症が1～2週間見られ，また，ウイルス血症に相前後して，糞便中へのウイルス排出が2～3週間見られる．E型肝炎はA型肝炎と同様，慢性化せず，肝硬変や肝癌への移行はない．終生免疫（一度感染すると二度目の感染や発症は阻止される）が成立するか否かは不明である．

本病は欧米や日本などの先進国では輸入感染症，すなわち，E型肝炎が常在している発展途上国への渡航者が罹患する疾病と考えられてきたが，近年，日本を含む先進国で海外渡航歴のないヒトでの本病の発生が確認された．また，HEVに対する抗体調査により，米国で1～5%，日本でも約5%のヒトが抗体陽性であることが明らかにされた．これらのことから，先進国でもHEVが土着しているのではないかと考えられるようになった．最近，ブタがHEVの保有宿主（レゼルボア）であり，また，日本において加熱不十分な野生動物肉などの喫食によりHEVに感染したと考えられる症例が幾つか報告された（後述）．

3．病原体

HEVは直径約30nmのエンベロープを持たない小型球形ウイルスで，約7.2Kbのプラス一本鎖RNAをゲノムとして持っている．1980年代初め，モスクワのBalayanがA型肝炎ウイルス陰性の流行性肝炎患者由来糞便抽出液を自ら飲み，肝炎の再現に成功した．これが本ウイルス発見の最初である．形態学的に食中毒の主要原因の一つであるノロウイルスと類似していること，主要な構造蛋白が一種であることなどから，以前はカリシウイルス科に分類されていた．しかし，ゲノム上での非構造蛋白機能ドメインの配置がカリシウイルス科のウイルスとは全く異なることが明らかとなり，現在は未分類のウイルスとされている．HEVが効率よく増殖する培養細胞系は確立されておらず，このことが，ウイルスの性状解析，本病の診断，また疫学調査を行う上で大きな障害となっている．HEVはゲノム塩基配列の相同性により，現在まで4種類の遺伝子型（Ⅰ～Ⅳ）に分けられている．発展途上国での流行ウイルスはⅠ型とⅡ型であるのに対し，先進国で海外渡航歴のないヒトからは主にⅢ型のウイルスが検出されている．また，中国と台湾での最近の散発的な発生は主にⅣ型であることが報告されている．このように発展途上国と先進国で検出されるウイルスの遺伝子型が異なり，人獣共通感染症の一面を持つと考えられる遺伝子型は主にⅢ型とⅣ型である．日本での検出例においても，海外渡航歴のないヒト症例からは主にⅢ型とⅣ型（北海道で多い）の検出が報告されている．地域的には北海道，東北および関東での症例が多く報告されており，現在までは「東高西低」の傾向がある．HEVは血清学的には単一と考えられ，実験感染において異なった遺伝子型のHEV間で交差防御が成立する．

4．診　　断

急性期患者の血清や糞便を検査材料としてRT-PCR法によるHEV遺伝子（RNA）検査が実施されている．現在広く使用されているプライマーは，いずれの遺伝子型（Ⅰ～Ⅳ）のHEV

も検出できるように設計されている．遺伝子型別はPCR産物の塩基配列の決定によって行われる．血清学的検査では，組換え蛋白を抗原としたELISA法が幾つかの機関で開発され，急性期と回復期のペア血清を用いたHEV IgG抗体価の上昇確認，また，急性期血清中のHEV IgM抗体の検出によって行う．

5．日本で確認されたHEVの感染ルート

日本おいてHEVが動物（食肉）からヒトに感染してE型肝炎を発症させたとする直接的あるいは間接的な証拠が2003～2004年に相次いで報告された（図6.1）．まず，北海道でヒトとブタから遺伝子レベルでほぼ同一のHEV（Ⅳ型）が検出された．また，北海道で市販の豚レバー363パッケージ中7件（1.9％）からHEV遺伝子（Ⅲ型あるいはⅣ型）が検出され，2001～2002年に北海道の特定病院で受診したE型肝炎患者（Ⅲ型あるいはⅣ型の感染）の多く（10名中9名）が発症2～8週前に加熱不十分な豚レバーを食べていたと報告された．また，鳥取県でイノシシの生肝臓を食べたヒト2名がE型肝炎を発症（Ⅳ型の感染）して内1名は死亡した．さらに，兵庫県においてシカの生肉を食べて肝炎を発症したヒト4名からとれたHEV（Ⅲ型）が食べ残しのシカ肉から検出されたHEVと遺伝子レベルで同一であったことが報告された．また，長崎県で老人会のイノシシ肉バーベキューパーティーにより12人中11人がHEV（Ⅲ型）感染し，内5人が発症した．加えて，北海道の焼き肉店で加熱不十分な豚レバーを摂取したと考えられる6名がHEVに感染し，内1名が劇症肝炎で死亡した．これらの証拠から，E型肝炎は人獣共通感染症としての側面を有することが明らかとなった．すなわち，これらHEVの感染ルートは食物性伝播（food-borne transmission）であり，動物由来感染（zoonotic transmission）であった．また，ウイルス保有宿主としてはブタ以外に野生動物も注目する必要が生じてきた．しかしながら，このようなルートによるヒトの感染はどの程

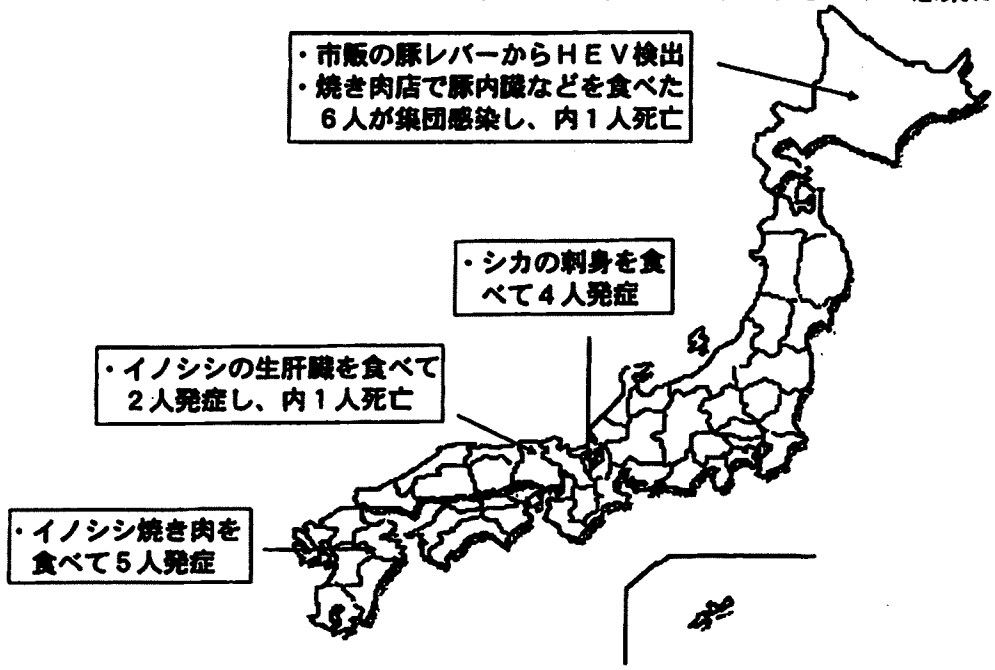

図6.1　2003～2004年に報告されたHEVの食物性伝播
（人獣共通感染症としての間接的ならびに直接的証拠）

度の頻度で起こっているのか，現時点では明らかではない．また，他の感染ルートとして，輸血による感染（blood-borne transmission）が2003年に報告されている．一方，北海道札幌市の特定病院で診断されたE型肝炎36症例においては，潜伏期間中での海外渡航歴は2例，輸血感染は見られず，聞き取り調査を実施した13例の中で食物性伝播の可能性は豚レバーを摂取した2例に留まったと報告されていることから，上記以外の感染ルートも存在すると考えられる．

6．ブタや他の動物でのHEV感染

ブタにおいてヒト由来HEVと遺伝子レベルで酷似したHEVが世界的に高率に浸淫していることが明らかにされている．ブタの血清，糞便，肝臓などからRT-PCR法によりHEV遺伝子が検出され，SPF豚からの検出例も報告されている．ブタから検出される遺伝子型はⅢ型とⅣ型のみであり，とくにⅢ型が多い．わが国のブタからも両型のウイルスが検出され，その多くはⅢ型である．

ブタにおけるHEVの感染時期に関して，血清中のHEV遺伝子は主に2～4カ月齢のブタから検出され，1カ月齢と6～7カ月齢以降のブタからは検出されなかったと報告されている．筆者らは糞便中のHEV遺伝子検査と血清中の抗体検査を実施した．その結果，糞便中のHEV遺伝子は2～3カ月齢のブタから高率に検出され，とくに，3カ月齢では検査した半数以上のブタが陽性を示した．また，検出率は低いが，出荷時のブタの糞便からも陽性例が確認された．血清中の抗体検査では，調査した31農場中30農場でHEVの浸淫が確認され，HEV陽性農場にはSPF農場も含まれていた．HEV陽性農場においては，抗体価の上昇は3～4カ月齢で顕著に認められ，4～5カ月齢では抗体陽性率が100％を示した（図6.2）．また，1980～1990年代に採取された豚血清も高率に抗体陽性を示した．これらのことから，HEVは日本のブタ集団に広く浸淫しており，SPF豚も例外ではないこと，ブタでのHEVの感染は2～3カ月齢が主であること，ブタのHEV感染はここ数年の間に急に広まったのではないことが明らかとなった．また，出荷時期の大部分のブタにおいてウイルスはすでに体内から消失しているが，一部例外も存在すると考えられた．

ブタにおけるHEVの病原性は低いと考えられる．豚由来株（Ⅲ型）のブタへの実験感染で

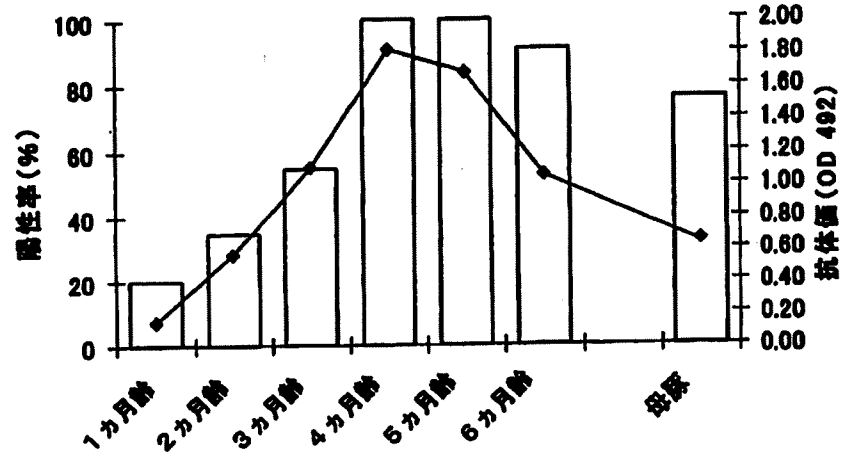

図6.2　ブタにおける月齢別HEV抗体陽性率（%；縦棒）と抗体価（OD値；折れ線）

は，肉眼病変として肝門リンパ節ならびに腸管膜リンパ節の腫大，組織病変としてリンパ球-形質細胞性肝炎と肝実質細胞壊死が認められるが，臨床症状やアラニンアミノトランスフェラーゼ（ALT；GPTとも呼ばれる）などの肝臓由来酵素の上昇は確認されていない．ウイルス遺伝子は肝臓，胆汁，糞便や血清などから2～3週間以上検出される．このようにHEVはブタにおいて浸淫率が高く病原性は低いことから，HEVの一部（Ⅲ型，Ⅳ型？）についてはブタが本来の自然宿主ではないかとも推測される．

ブタ以外の哺乳動物においてHEV遺伝子は，シカ，イノシシおよびマングースから検出されている．また，HEV抗体は，ラット，ウシ，サル，ヒツジ，ヤギ，ネコ，イヌ，イノシシなどで確認されている．よって，ブタ以外の動物においても，HEVあるいはHEV様ウイルスの感染があると考えられるが，これらの感染実態はほとんど不明である．一方，トリにおいては，ヒトHEVと抗原交差するが，遺伝学的には明らかに区別されるウイルス（big liver and spleen disease virus，トリHEV）が検出されている．

7．動物からヒトへのHEVの伝播

ブタからヒトにHEVが伝播する直接証拠は現在まで報告されていない．しかし，前述のように加熱不十分な豚レバーを食しての感染を示唆する報告があるほか，多くの研究者がブタ-ヒト伝播の可能性を指摘している．その根拠は大きく以下の三点に基づいている．第一点目はウイルス遺伝子の近似性である．先進国において海外渡航歴のないヒトとブタから主に検出されるHEVはどちらもⅢ型である．一方，台湾と中国では最近のヒトでの主要なHEVはⅣ型であり，両国のブタから検出されるHEVは同じⅣ型である．また，同じ遺伝子型の中でも，地理的に近い地域から検出されたブタ由来株とヒト由来株は，地理的に遠い地域からのそれらよりも遺伝学的により近縁である場合が多い．さらに，前述のようにヒトとブタから遺伝学的にほぼ同一のウイルスが検出されている．第二点目の根拠として，一部のHEVはサルとブタの両方で実験感染が成立することがあげられる（表6.1）．ヒト由来株Ⅰ型，Ⅱ型，Ⅲ型はいずれもサルへの接種により感染が成立する．一方，ヒト由来株Ⅰ型あるいはⅡ型をブタに接種した場合，ブタは感染しない．しかし，Ⅲ型のヒト由来株をブタに接種すると感染は成立し，また，Ⅲ型のブタ由来株をサルに接種しても感染する．すなわち，Ⅲ型のHEVは種を超えて感染することが明らかにされている．第三点目の根拠は，ブタと頻繁に接触するヒトと，全く接触しないヒトでHEV抗体陽性率が異なるという

表6.1　HEVを実験的投与されたサルとブタでのHEVの感染性

遺伝子型	由来	株名	感染性[a]	
			サル	ブタ
Ⅰ	ヒト	Sar-55	○	×
Ⅱ	ヒト	Mex-14	○	×
Ⅲ	ヒト	US-2	○	○
Ⅲ	ブタ	swUS1	○	○

[a] ○，感染性有り；×，感染性無し

表6.2　ブタに頻繁に接触するヒトと全く接触しないヒトとのHEV抗体陽性率の比較

調査国	調査年	比較対象	陽性数/検査数	HEV抗体陽性率（%）
台湾[a]	1999	養豚従事者	8/30	26.7
		豚肉取扱者	3/20	15.0
		豚非接触者	4/50	8.0
モルドバ[b]	2001	養豚従事者	135/264	51.1
		豚非接触者	63/255	24.7
米国[c]	2002	養豚従事者	18/165	10.9
		豚非接触者	3/127	2.4
米国[d]	2002	豚専門獣医師	78/295	26.4
		豚非接触者	73/400	18.3

[a] Hsieh *et al.* (1999) J Clin Microbiol 37 : 3828-3834
[b] Drobeniuc *et al.* (2001) J Infect Dis 184 : 1594-1597
[c] Withers *et al.* (2002) Am J Trop Med Hyg 66 : 384-388
[d] Meng *et al.* (2002) J Clin Microbiol 40 : 117-122

成績による（表6.2）．台湾での抗体陽性率は養豚従事者26.7％，対照者8％，モルドバでの陽性率は養豚従事者51.1％，対照者24.7％，米国ノースキャロライナ州においては，養豚従事者10.9％，対照者2.4％と報告されている．また．米国8州でのブタ専門獣医師の抗体陽性率は26.4％，対照者のそれは18.3％と報告されている．このように，いずれの報告においても頻繁にブタと接触するヒトは非接触者に比べて抗体陽性率が高い結果となっている．

ブタ以外の動物からヒトへのHEVの伝播は，前述のように，加熱不十分な野生動物の内臓や肉の喫食によると考えられる例が報告されている．ごく最近，シカ肉の生食によるHEV感染のリスクが評価された．この報告によると，日本の一地域においてシカ肉生食経験者の血清中HEV抗体陽性率は17.7％，一方，同じ地域でのシカ肉生食未経験者（対照者）のそれは2.2％と有意な違いが認められている．

8．治療・予防対策

治療は対症療法のみであり，劇症肝炎には，血漿交換，人工肝補助療法，肝移植などが必要となる．

E型肝炎のワクチンは現在開発段階である．輸入感染症としての本病の予防は，本病常在国への渡航時には清潔の保証がない飲料水，非加熱の貝類，自分自身で皮をむかない非調理の果物・野菜を摂取しないようにする必要がある．

動物（食肉）に起因するE型肝炎発生のリスクについては不明な点が多い．とくに，野生動物におけるHEVの感染実態はほとんど明らかにされておらず，早急な調査が必要とされる．一方，HEVはSPF豚を含めた豚集団に高率に浸淫しているが，養豚従事者に肝炎発症者が多いという事実は現在まで確認されていない．このことは，ブタとの日常的な接触に

よってE型肝炎を発症するものではないことが想定されるが，結論にはさらなるデータの蓄積が必要である．また，HEV感染の回避だけでなく，養豚における基本的な労働衛生管理として，ブタ接触後の手洗いの励行と衣服や履物の交換は大変重要である．一方，農場においては，適切な糞尿処理を実施して流出や地下浸透による水質汚染のないようにする必要がある．

ブタにおけるHEVの主な感染時期は育成期であり，大多数のブタは出荷時にはすでに感染耐過してHEVは体内から消失していると考えられる．しかし，一部の出荷豚の糞便や市販の豚レバーからHEV遺伝子が検出されていることから，内臓や筋肉にHEVが含まれるリスクはゼロでない．このため，レバーなどの内臓肉だけでなく正肉も含めて生食は行うべきではない．生食を行わないことは野生動物の肉などにおいても全く同様である．HEVは通常の「加熱調理」により感染性を失うため，肉や内臓を食べることによる感染の危険性はなくなる．ブタにおいて日齢の違いによりHEVに対する感受性が異なるという報告は現在まで見当たらない．一方，成豚でのHEVの実験感染例が報告されている．このことから，現状の感染時期はブタの飼育方法や飼育環境が大きく影響していると考えられ，これらが変化すると感染時期が変わる可能性は残されている．よって，農場毎にHEVの感染実態を定期的に調査することも今後必要であると考える．

参考文献

1) Meng XJ (2003) Swine hepatitis E virus : cross-species infection and risk in xenotransplantation. Curr Top Microbiol Immunol 278 : 185-216.
2) Meng XJ, Purcell RH, Halbur PG, Lehman JR, Webb DM, Tsareva TS, Haynes JS, Thacker BJ, Emerson SU (1997) A novel virus in swine is closely related to the human hepatitis E virus. Proc Natl Acad Sci USA 94 : 9860-9865.
3) Okamoto H, Takahashi M, Nishizawa T (2003) Features of hepatitis E virus infection in Japan. Intern Med 42 : 1065-1071.
4) 武田直和 (2004) E型肝炎. 感染症の話. IDWR感染症週報. http : // idsc. nih. go. jp / kansen / index. html
5) Tei S, Kitajima N, Takahashi K, Mishiro S (2003) Zoonotic transmission of hepatitis E virus from deer to human beings. Lancet 362 : 371-373.
6) White DO, Fenner FJ (1996) E型肝炎. 医学ウイルス学.. 北村　敬訳. 367-369. 近代出版. 東京.

恒光　裕（動物衛生研究所 ウイルス病研究チーム　Hiroshi Tsunemitsu）

Arch Virol (2009) 154:1263–1269
DOI 10.1007/s00705-009-0433-6

ORIGINAL ARTICLE

Characterization of anti-idiotypic antibodies mimicking antibody- and receptor-binding sites on hepatitis A virus

Tomoko Kiyohara · Atsuko Totsuka · Tetsuo Yoneyama · Koji Ishii · Toshihiro Ito · Takaji Wakita

Received: 19 December 2008 / Accepted: 12 June 2009 / Published online: 4 July 2009

Abstract Two anti-idiotypic monoclonal antibodies (mAb2s; named 94-2 and 94-7), were generated from a BALB/c mouse immunized with human monoclonal anti-hepatitis A virus (HAV) neutralizing antibody KF94. We characterized the properties of the mAb2s and determined interactions between mAb2s, KF94 and HAV using enzyme-linked immunosorbent assay, immunofluorescence assay and HAV infectivity assay. Inactivated HAV inhibited mAb2 binding to KF94, indicating that the mAb2s mimicked the HAV neutralization site that was complementary to the paratope of KF94. MAb2 94-7 competed with an anti-HAV cellular receptor antibody for binding to HAV-susceptible cells and partially blocked virus infection. We speculated that mAb2 94-7 mimicked a portion of the HAV receptor-binding site. The ability to generate mAb2 implies that HAV receptor-binding sites are exposed on the surface of HAV, permitting antibody access.

Introduction

Hepatitis A virus (HAV) is an epidemiologically important pathogen that causes acute hepatitis in humans [12]. It is a positive-strand RNA virus belonging to the family *Picornaviridae*, genus *Hepatovirus* [16].

Picornavirus particles contain 60 protomers arranged as 12 pentamers. Each protomer is composed of four capsid proteins, viral protein (VP) 1, VP2, VP3 and VP4. The HAV particle also contains 60 protomers, made up of the same capsid proteins, but the VP4 of HAV is truncated and smaller than the VP4 proteins found in other picornaviruses [5].

Unlike other picornaviruses [3], the antigenic structure of HAV has not been completely characterized. Its unique features, the difficulty of obtaining a high virus yield in tissue culture and the strict conformational dependence of its own neutralizing antigenic structure have hampered investigations of HAV morphology. Generating neutralizing antibodies in response to individual structural proteins, synthetic peptides or expressed polypeptides is reportedly difficult [7, 10, 15]. Fragmental structural proteins cannot maintain the function of the neutralizing site. Studies using escape mutants have generated information about the antigenic structure of HAV [17, 19] that supports the notion of an immunodominant neutralizing site involving residues of VP1 and VP3, and that a second, potentially independent site involves residue 221 of VP1.

We generated anti-idiotypic antibodies (anti-Id) by immunization with an HAV-specific human neutralizing monoclonal antibody to investigate the antigenic structure of HAV. Immunization with an antibody (Ab1) can induce anti-antibody antibodies (Ab2s), and those specific for idiotopes of Ab1 are considered anti-Ids. Idiotopes are confined to the variable region of immunoglobulin molecules, and they are crucial for antigen recognition [21]. Among the four known types of anti-Ids (Ab2α, Ab2β, Ab2γ and Ab2ε) [2], Ab2β binds directly to the

T. Kiyohara (✉) · A. Totsuka · T. Yoneyama · K. Ishii · T. Wakita
Department of Virology II, National Institute of Infectious Diseases, 4-7-1, Gakuen, Musashi-Murayama, Tokyo 208-0011, Japan
e-mail: kiyohara@nih.go.jp

T. Ito
Laboratory of Veterinary Public Health, Faculty of Agriculture, Tottori University, 4-101, Minami Koyama, Tottori 680-8553, Japan

idiotope within the paratope of Ab1. Ab2β has the potential to mimic the structure of the antigenic epitope complementary to the Ab1 paratope and it has an antigen-like function. Several reports have used anti-Ids to identify viral/bacterial antigenic structure or cellular receptors [1, 9].

Here, we describe the properties of our anti-Ids, designated mAb2 94-2 and 94-7, which mimic the HAV surface structure and allowed unique insight into the antigenic structure of HAV.

Materials and methods

Cell line and viruses

The GL37 line was derived from African green monkey kidney cells and established to support the optimal growth of HAV [20]. GL37 cells were cultured in Eagle's minimal essential medium (Nissui, Tokyo, Japan) supplemented with 50 μg/ml of gentamicin (Biological Industries, Kibbutz Beit Haemek, Israel) and 10% fetal bovine serum (FBS, GIBCO, Invitrogen Corporation, Auckland, NZ).

Human tissue-culture-adapted hepatitis A virus strains KRM003 (genotype IIIB), KRM031 (genotype IA) and TKM005 (genotype IB) were isolated from patients with hepatitis A [18] and propagated in GL37 cells. Each strain was purified from cell extracts by differential centrifugation, chloroform extraction, RNase, DNase and protein K digestion, extraction with a mixture of 2-ethoxyethanol and 2-buthoxyethanol, and gel filtration. After sucrose gradient centrifugation, the fraction containing intact particles was selected.

The HAV strain KRM003 was propagated and purified as described above. Purified virus was inactivated with 0.025% formalin at 37°C for 12 days and then diluted with 10 mM Tris–HCl, 2 mM EDTA, 100 mM NaCl, 0.02% Tween 80, 0.1% NP40, 0.2% BSA, 0.03% NaN_3 to 3 mg/ml and stored at 4°C.

Preparation of anti-HAV antibodies

Syngeneic anti-HAV human monoclonal antibodies designated KF6 and KF94 provided by Dr. Yasushi Kuwahara, Denka Seiken Co. Ltd. [4] corresponded to Ab1s derived from the blood of a convalescent patient with hepatitis A who was infected with strain IIIB. Here, the parental antibody was KF94, which cross-reacted with a mouse monoclonal antibody that recognized the HAV immunodominant site (data not shown).

Anti-HAV rabbit hyperimmune serum was prepared by immunization with the inactivated HAV.

Generation of mouse monoclonal anti-KF94 antibodies (mAb2s)

Hybridoma clones were selected from the fusion products of SP2/0 myeloma (Riken Cell Bank, Tsukuba, Japan) and spleen cells of BALB/c mice immunized with KF94.

The affinity of culture fluid from each hybridoma clone to KF94 was tested using an enzyme-linked immunosorbent assay (ELISA) (Table 1). Polystyrene microtiter plates (F96 CERT. MAXISORP, Nunc Laboratories, Roskilde, Denmark) were coated with 50 μl of appropriately diluted KF94, or with anti-HAV-negative human serum obtained from a healthy individual. Sera or specimens derived from human sources were collected after obtaining informed consent from the donors.

Nonspecific binding in the wells was blocked with bovine serum albumin. Culture fluid (50 μl) was applied to plates coated with either KF94 or anti-HAV-negative human serum. Bound antibody was detected by incubation with a horseradish-peroxidase-conjugated (HRPO) anti-mouse IgG (MBL, Nagoya, Japan) followed by *o*-phenylenediamine (Tokyo Chemical Industry Co, Ltd, Tokyo, Japan) substrate. Thirty minutes later, the reaction was stopped with 2 N H_2SO_4. Absorbance was measured at 492 nm in an ELISA plate reader (Corona, Hitachinaka, Japan). The procedures for color development and absorbance measurement subsequent to adding conjugated antibody were identical in every subsequent ELISA.

Antibodies that reacted with KF94 and not with anti-HAV-negative human serum were identified as KF94-specific mAb2s. The isotype of the mAb2 was determined using a mouse monoclonal antibody isotyping test kit (Serotec Ltd., Oxford, UK). The ascitic fluid of each mAb2 was obtained by intraperitoneal injection of hybridomas into pristane-primed BALB/c mice. Animals were handled and cared for in accordance with the "Guidelines for Animal Experimentation at NIID."

Cross-reactivity between the selected mAb2s was determined by competitive inhibition ELISA using biotin-labeled mAb2s and KF94-coated plates (Table 1). Briefly, non-labeled mAb2 was applied to KF94-coated plates, followed by biotin-labeled specific or non-specific mAb2. The mAb2 was labeled with biotin using EZ-Link NHS-Biotin (Pierce, Rockford, IL, USA) according to the manufacturer's instructions and detected using HRPO avidin (MBL, Nagoya, Japan).

Biotin-labeled mAb2s were also used in mAb2-HAV binding ELISA (Table 1). Serially diluted biotin-labeled mAb2s were applied to plates that were prepared as follows: polystyrene microtiter plates were coated with 50 μl of anti-HAV rabbit hyperimmune serum, and nonspecific binding was blocked with bovine serum albumin. Fifty microliters of formalin-inactivated HAV strain KRM003

Table 1 Summary of ELISA used in this study

Aim of ELISA	Plate coated with	First input	Second input	Third input
MAb2-KF94 binding	KF94	MAb2	HRPO anti-mouse IgG	–
MAb2 cross reactivity	KF94	MAb2	Biotin-labeled mAb2s	HRPO avidin
MAb2-HAV binding	Anti-HAV rabbit hyperimmune serum[a]	Inactivated HAV	Biotin-labeled mAb2s	HRPO avidin
Inhibition of binding of Ab1 to HAV by mAb2	Anti-HAV rabbit hyperimmune serum[a]	Inactivated HAV	The mixture of Ab1 and mAb2	HRPO anti-human IgG
Inhibition of binding of KF94 to mAb2 by HAV	KF94	Inactivated HAV	Biotin-labeled mAb2s	HRPO avidin
Competitive inhibition	GL37 cells	MAb2s	HRPO anti-HAV receptor antibody 190/4C	–

[a] We confirmed that anti-HAV rabbit hyperimmune serum did not bind to mAb2s

(20 ng/ml) was added, and the plates were incubated overnight at 4°C. Bound biotin-labeled mAb2s were detected as described above.

Inhibition assays

We determined the ability of the mAb2 to inhibit the binding of KF94 to HAV (Table 1). A mixture of diluted Ab1 and mAb2 was incubated at 4°C overnight and then applied to HAV-coated plates. Bound Ab1 was detected using a HRPO anti-human IgG (Dako, Glostrup, Denmark).

We examined the ability of inactivated HAV to inhibit the binding of KF94 to mAb2 (Table 1). Serially diluted inactivated HAV was incubated in KF94 plates overnight at 4°C, and then the wells were emptied. Biotin-labeled mAb2 (diluted 1:1,000) was applied to the wells, followed by HRPO avidin. Inhibition rates were measured using the formula:

Inhibition rate (%) = 100 × (absorbance without inhibitor − absorbance with inhibitor)/absorbance without inhibitor.

Anti-HAV-cellular-receptor mouse monoclonal antibodies

Anti-HAV-cellular-receptor mouse monoclonal antibodies (anti-HAV-receptor antibodies), designated 190/4, 235/4 and 263/6, were induced by immunizing GL37 cells and selected by their ability to block HAV propagation in GL37 cells [11]. We confirmed that the anti-HAV receptor antibodies recognized a common receptor. Anti-HAV receptor antibody190/4 was conventionally conjugated with horseradish peroxidase and named 190/4C.

Binding of mAb2 to HAV cellular receptor

The binding of each mAb2 to GL37 cells was examined using an immunofluorescence assay. The positive controls were the anti-HAV-receptor antibodies, 190/4, 235/4 and 263/6, and the negative control was a normal mouse serum (NMS) that was confirmed to be negative for anti-HAV antibody.

Confluent, unfixed GL37 cell monolayers on glass cover slips were gently washed with phosphate-buffered saline (PBS) and then incubated with mAb2 or control antibodies for 1 h at 37°C in a moist chamber. The cover slips were washed with PBS and then incubated with fluorescently labeled anti-mouse IgG (MBL, Nagoya, Japan) for 1 h at 37°C in a moist chamber. The labeled anti-mouse IgG was removed, and the cover slips were washed three times in PBS. The cell surface was immediately observed using a fluorescence microscope.

We confirmed using competitive inhibition ELISA that mAb2 94-7 and anti-HAV receptor antibody 190/4 shared the same HAV cellular receptors.

The anti-HAV receptor antibody 235/4 was the positive competitor, and an anti-human Fc mouse monoclonal antibody (anti-human Fc mAb) was the negative competitor in this ELISA. An anti-human Fc mAb bound non-specifically to KF94 despite being simultaneously generated with the mAb2s 94-2 and 94-7.

Confluent GL37 cell monolayers in 96-well cell culture plates (Corning, NY, USA) were incubated with serially diluted mAb2s and positive or negative competitors for 2 h at 37°C. After washing with PBS, 50 µl of HRPO anti-HAV-receptor antibody 190/4C was added to the corresponding wells and incubated for 2 h at 37°C. The wells were washed, and then bound HRPO anti-HAV receptor antibody was detected. Competition rates were measured using the formula:

Competition rate (%) = 100 (absorbance without competitor − absorbance with competitor)/absorbance without competitor.

Infectivity assays

We performed $TCID_{50}$-infectivity and immunofocus assays to investigate the mAb2-mediated protection of GL37 cells against HAV infection.